A DISCRETE ELEMENT APPROACH TO PREDICTING THE UNIAXIAL COMPRESSIVE RESPONSE OF PLAIN CONCRETE

by

Nakul Sharad Tannu

A thesis submitted to the faculty of
The University of North Carolina at Charlotte
in partial fulfillment of the requirements
for the degree of Master of Science in
Mechanical Engineering

Charlotte

2017

Approved by:

Dr. Harish P. Cherukuri

Dr. Miguel A. Pando

Dr. Ronald E. Smelser

ABSTRACT

NAKUL SHARAD TANNU. A discrete element approach to predicting the uniaxial compressive response of plain concrete. (Under the direction of DR. HARISH P. CHERUKURI and DR. MIGUEL A. PANDO)

Discrete element method (DEM) has become the method of choice for modeling the mechanical response of materials with granular structure. The method consists of representing the material as a collection of particles that interact with each other by transmitting forces through contact between neighboring particles. In DEM, the particles are typically idealized as rigid and the contact forces and associated deformations are modeled through spring-damper systems between the contact particles with various degrees of sophistication and complexity including particle bonding and cohesion necessary for concrete materials. The deformations due to contact include normal displacements as well as tangential displacements. The tangential forces can cause rolling, sliding as well as torsion. For bonded particles, the normal forces can be tensile or compressive. The normal and tangential responses due to applied forces or displacements are controlled by a multitude of user-specified parameters such as the damping coefficients, normal and tangential stiffnesses, tensile and compressive strengths and geometric factors such as the size and shape of the particles, as well as the number and packing arrangement of the particles.

This thesis consists of two parts. In the first part, a parametric study of two-particle and three-particle systems was conducted to understand the effect of various DEM parameters on the system response. The DEM component of the commercial finite element software package LS-Dyna was used for the numerical simulations. The

parallel-bond contact model was used for capturing the interaction between the particles. The second part of the thesis consists of modeling the uniaxial compressive response of an unreinforced concrete cylinder using a dense packing of spherical particles coupled by parallel-bonds. Guided by the results of the first part, the sensitivity of the predicted results for concrete response to particle size and influence of various parallel-bond parameters on the bulk response was studied to produce a calibrated model that shows to be capable of producing realistic uni-axial compressive behavior as observed in experiments. The results show that the maximum compressive stress in the concrete cylinder largely depends on the strength of parallel bonds and initial particle arrangement or sample void ratio. The axial strain to failure, as predicted by the DEM model considered, is largely dependent on the bond modulus and to a lesser extent on the particle size. Unlike other numerical techniques, particle size does not act as a free parameter that controls resolution; however, for uni-axial compression problem it affects the overall damage process.

DEDICATION

To my parents,

Sharad Tannu and Ujwala Tannu

And my loving sister,

without whom none of my success would be possible.

ACKNOWLEDGMENTS

I would like to thank my advisors, Dr. Harish Cherukuri and Dr. Miguel Pando for their excellent guidance and motivation. I heartily appreciate Dr. Cherukuri for his encouragement throughout this project and for imparting a truly professional learning experience. I would like to thank Dr. Pando for the valuable inputs during group meetings and his support in the present work. I genuinely acknowledge his support and guidance. I would also like to thank Dr. Ronald Smelser for being a part of my thesis committee and for his valuable suggestions and inputs.

I would like to thank every member of my research group for their constructive critique to make this work more presentable. I would like to thank my dear friend and colleague Jaimeen Patel and my roommate Rumit Gajera for their support, encouragement and valuable inputs throughout my research. Finally, I would like to thank all the faculty and staff of the Department of Mechanical Engineering and Engineering Sciences at UNC Charlotte that helped and contributed to the completion of my MS degree and this thesis.

TABLE OF CONTENTS

LIST OF FIGURES

LIST OF TABLES

CHAPTER 1: INTRODUCTION

1.1 Background

The discrete element method (DEM) is a numerical technique that has become the method of choice for studying the mechanical response of materials with granular structure at multiple scales. DEM models can be used to study breakage and fracture location and also to predict macroscale response of a large variety of materials. The method requires several input parameters that characterize the interaction between the particles in addition to the specification of distribution of the particle sizes and time-step size. In this thesis, the DEM is used to study the effect of many of these parameters on the response of a few elementary DEM systems followed by an application of the method to study the uniaxial compressive response of plain (unreinforced) concrete. This section provides some background information on concrete, and the discrete element method.

Concrete is the most commonly used man-made material in the world, and consists of cementitious man-made material composed of cement, gravel, and water. Concrete has been reported as being used in construction by Egyptians as early as 1950 B.C. [2]. The widespread use of concrete today in the modern world is primarily due to its high compressive strength to cost ratio. A dditionally the main constituents of concrete can be easily varied to modify its overall strength, durability and other

properties.

The uni-axial compressive behavior of concrete materials can be studied mainly with three different approaches: physical testing, analytical methods, and numerical techniques. Use of the physical tests is the most reliable and trusted approach. The applicability of these experiments accounts for several drawbacks and limitations. It is often the preferred approach in construction QA/QC, however cost and other drawbacks may sometimes limit its use. Analytical methods are also popular to predict the response of concrete structures due to various loads. This approach often involves use of equations that are derived from empirical correlations and are limited in their applicability and thus, the method has to be used with caution.

The third approach is to use numerical methods. Numerical methods are relatively easy to implement and more flexible than physical testing. The advantage of computer simulations is that it has the flexibility to allow variation of different input parameters and to investigate sensitivity of key variables which allows precise control over the predicted material properties. It also allows study of the breakage process that can be carefully observed as the crack-producing flaws progresses, this crack propagation is expensive to replicate experimentally as the actual process occurs very rapidly and requires specialized imaging techniques [25]. Numerical models are based on the concept of representation of the material that in general can be either continuous mass or discrete/granular particles. Numerical modeling of cementitious material like concrete can be done using either continuous or discrete models.

Numerical studies of the uniaxial compressive behavior of plain concrete using continuum-based methods such as the finite element (FE) method have been very

popular since the development of FE methods for the past 67 years [1]. Most commercial FE software packages include nonlinear constitutive models for concrete behavior (LS-Dyna, ABAQUS, PLAXIS). Although FE is a popular approach to predict mechanical behavior of concrete, modeling of fracture of heterogeneous solids is a difficult problem to solve numerically, due to the creation of continuous motion of new surfaces [17]. Also in conventional FE methods element distortion is a major concern due to large displacements in granular materials like concrete.

In contrast, the discrete approach using DEM is much more recent. The DEM approach has the advantage over the FE continuum approach in that it can relatively better capture the mechanical behavior of an inherently discrete material such as concrete. DEM was first proposed by P. A. Cundall for studying large-scale movements in blocky rock system [7]. This approach was later studied and subsequently used to develop a bonded particle model for rock (BPM) by D.O. Potyondy and P.A. Cundall [26]. In this thesis, the bonded particle model forms the basis for studying the response of Concrete under uniaxial compression.

1.2 Literature review

DEM is considered to be computationally more expensive relative to other numerical techniques. However, with the increase in computational power in last two decades, DEM has been a popular choice in various areas such as geotechnical engineering, mining, civil engineering, powder metallurgy, chemical engineering, pharmaceutical, and food handling industries. The method continues to grow in popularity due to advances in computing power and numerical algorithms for nearest neighbor

searching, that have allowed DEM models to numerically simulate millions of particles on a single processor [33]. This increased ability makes DEM more suitable for simulating structures consisting of a large number of particles like soil, grains, and masonry structures. The use of DEM technique first started with the study of earth materials by Cundall & Strack [9] who explored the study of granular media with no cohesion. Liu et al. [18]; Yao & Anandarajah [31] examined DEM models of soil with cohesion, Rock problems modeled with DEM have been reported by Moon et al. [21]; Potyondy & Cundall [26]. Similarly DEM applied to asphalt has been described by You et al. [32].

In the context of soil with cohesion, cohesion is defined as a weak bond between two particles due to the surface tension of water molecules. Typically, cohesion is used in modeling of wet soil accompanying with shear tests and biaxial tests. Tsuji et al. [29], studied the soil moisture condition using liquid bridges between particles and measured connections between bulldozer blade and soil.

The study of earth-moving machines, involving analysis of tool-rock interfaces, often requires hybrid finite-discrete element numerical techniques to accommodate large displacements of a granular material and the relatively small deformation of the tool. B. Aresh [3] studies the mechanics of material removal in rock cutting using ELFEN; a hybrid finite-discrete element commercial package. J. Rojeck [27] discusses the modeling of rock cutting using DEM, while the tool is represented as a rigid body.

For a numerical technique to qualify as a discrete element method, Cundall and Hart define essential elements that a DEM numerical scheme must posses, as the following [8]:

- Must recognize new contacts automatically as the calculation progresses.
- Must allows finite displacements and rotations of discrete bodies, including complete detachment.

The numerical scheme will be limited to small numbers of bodies as the interactions are known in advance and no new contacts are automatically detected. The second element is important otherwise a DEM numerical scheme will fail to reproduce some important mechanisms in a discontinuous medium, including damage development within the body.

A discrete element model is made up of two basic components: the elements and the contacts between them. The elements can represent individual physical units of the analyzed system or collections of the individual units. The elements can have different shape, sizes and distribution over the domain. From a computational point of view circular for 2D and spherical in 3D elements are the easiest to handle [13]. Depending on the application and contact model used, the elements can be either perfectly rigid or deformable. An element is said to be in contact when the distance between two elements - suitably defined - is zero. However, a distance less than zero represents an overlap between the two elements, and the magnitude of the overlap defines a compressive force acting on them. Frictional force, tangential and normal stiffness, damping coefficient are then incorporated within the elemental contacts to model the overall bulk behavior. Other contact forces such as bending moment, tension and torsion are possible using the Bonded Particle Method (BPM), which serves as a major contribution to the behavior of cementitious materials like concrete.

1.2.1 Bonded particle models in DEM

Different bonded particle models exist today like those proposed by Schneider et al. [28] and Potyondy and Cundall [26]. These have been developed and implemented in various DEM software, e.g., LS-Dyna (Livermore Software Technology Corporation), EDEM (DEM Solutions Ltd), Particle Flow Code (PFC) (Itasca Consulting Group), and DEMPack (CIMNE Edifici). The four features that most packages share and which influence the way Bonded Particle Method is modeled are listed as follows:

- Particle generation and distribution
- Initialization of bonds
- Contact model
- Bond failure

Each of these features are discussed in detail in the following subsections.

1.2.2 Particle generation and distribution

As the feature name implies, a collection of particles representing the subject material is created. Particle sizes are user specified and many packages allow for nonuniform particle sizes and multiple shapes of the particles. In the present work, the particle shape is restricted to spherical. Thus an element corresponds to a spherical particle for this study. The approach is to model the geometry with discrete particles as close as elements corresponding to the units of real structure. In the cases of sand, soil and concrete, several thousands of densely packed particles that represent a huge

number of real particles, have to be defined randomly. There are several particle generation techniques used in DEM simulation. A brief description of three of the most widely used techniques is presented below (Z. Gyurko [13]).

1. *Dynamic techniques*: The elements initially located far from each other or randomly generated at a user defined planer surface usually known as particle generation factory surface and are pushed into a significantly denser arrangement by gravity or isotropic compression. A closed domain may not be necessary however a domain of the required geometry shape may be required for the particle rearrangement. Figure 1a shows the generation of particles from top factory surface while particles are allowed to arrange themselves due to gravity. This method is computationally expensive as a DEM solution is required and new elements are generated simultaneously.

2. *Constructive algorithms*: These algorithms are purely based on geometrical calculations. LS-Dyna uses advancing front approach [11] to generate particles in a closed domain. With the advantage that no secondary rearrangement is required, these algorithms are more efficient than dynamic techniques. In this method, the spheres of given diameters, specified by the user, are placed at specific positions, using advancing front algorithm, in the domain of interest. The algorithm ensures that no newly placed particle intersects with a previous one, if any intersection or overlap is detected, then the new particle is rejected, and the algorithm places the particle into another part of the domain. This process runs until the algorithm returns a high number of unsuccessful tries.

When no further particle is accepted in the domain, the domain is considered as completely filled. Since this method requires a closed domain to be specified, element generation in bulk for open geometries, like flow over a conveyor belt, is not possible. Figure 1b shows a rectangular domain filled using advancing front approach.

3. *Collective rearrangement techniques*: In these methods, for a specific domain, the user defines a fixed total number of particles during the sample preparation process. A closed domain may be required for models having complex shapes. At the first step, all the particles are placed randomly and overlaps are allowed within elements. The next step during the process is to displace all the particles in contact equal to the amount of their overlap. Since this method is a two-step process, collective rearrangement techniques similar to dynamic methods, are rather time-consuming. Figure 1c shows a representation of collective rearrangement technique.

For a cementitious material like concrete, the size of each particle and the total number of particles in an actual material is a fundamental phenomena for accurately modelling a model to be studied. It is highly impossible to represent each individual grain of actual material with a discrete particle. However, it is important that there is a sufficient number of elements in a simulation to ensure a high enough resolution to study material behavior.

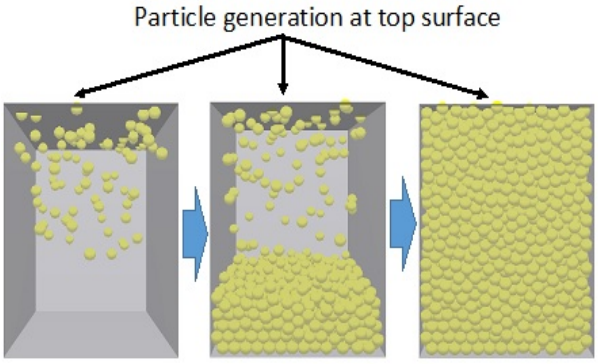

(a) Dynamic technique

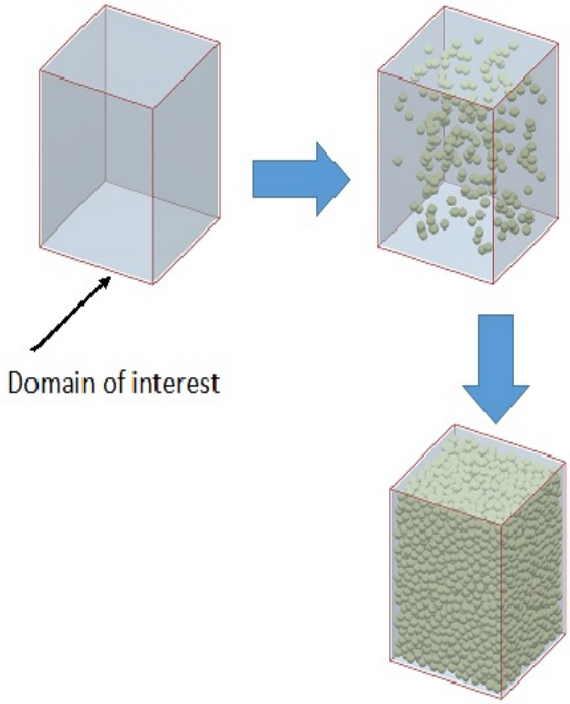

(b) Constructive algorithm

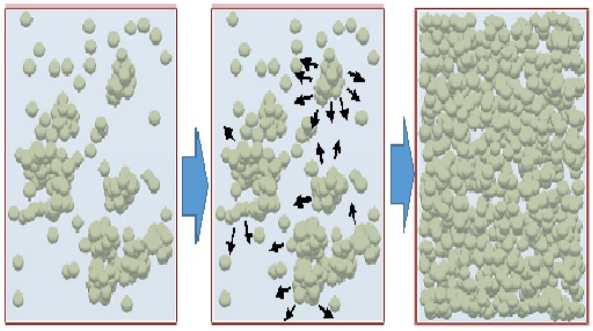

(c) Collective rearrangement techniques

Figure 1: Particle generation techniques.

In the case of concrete materials, this will relate to the size of cracks that can develop. The particle size distribution for spherical particles can be divided into three categories as follows:

1. Mono-disperse: This uses one size of particle for the entire sample [30].

2. Bi-disperse: This uses two sizes of particle for the entire sample [6].

3. Poly-disperse: This uses multiple sizes of particle for the entire sample [23].

1.2.3 Initialization of bonds

Bond models differ from non-bonded DEM models by the inclusion of a mechanism that represents the cement joint between grains found in cementitious materials. A specific criterion is required to form a bond between two particles. For example, the maximum distance between the two particles is commonly used as a bond formation criterion. If neighbouring particles are at a distance equal to or less than this specified maximum distance the bonds will be formed. These bonded contacts can then be treated accordingly to calculate relative resisting forces unlike a non-bonded contact. If the value of the parameter that defines the bonding criteria is reduced, the number of bonds will reduce, and so the material being represented will behave more granular in nature [10]. The BPM model requires the geometric dimensions of the bond to calculate the force-displacement law for a single bond between two particles. For spherical particles, the bond is assumed to be a cylinder of uniform cross section. The length of the bond is taken as the straight line distance between particle centres.

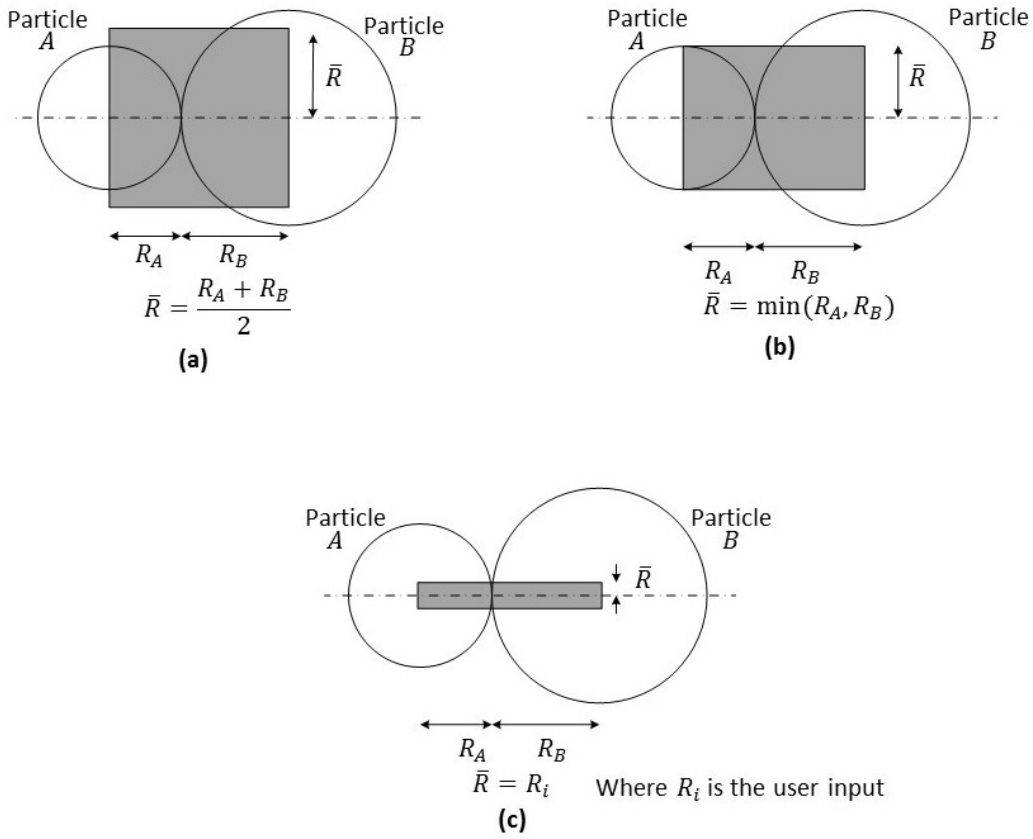

Figure 2: Methods in determining the cross sectional geometry of a bond. (a) Arithmetic mean of particle radii, (b) Minimum particle radius, (c) Harmonic mean of particle radii. (Adapted from [5])

Shown in Figure 2 the three widely used methods to determine the radius of the bond are:

1. Arithmetic mean of particle radii.

2. Minimum particle radius.

3. User input value.

1.3 Thesis objectives

The objectives of the present study are as follows:

1. To analyze the influence of parallel-bond parameters on material macro-properties. For this purpose, elementary systems involving only two and three particles are considered..

2. To develop a 3D DEM model for concrete cylinder under uni-axial compression test.

3. To Initialize bonds between the particle of the model using the BPM method.

4. Using quantitative data of simpler models, calibrate the 3D model to the desired strength.

5. To validate and verify the numerical stress-strain curves with known experimental data.

6. To calculate the numerical lateral and axial strains and calculate volumetric strain of the model.

7. To analyse the overall damage and fracture patterns predicted by the DEM models.

1.4 Organization of thesis

The rest of the thesis is divided into six chapters as follows. Chapter 2 presents a general background on the working of DEM. The theory of non-bonded as well as bonded contact models are described in detail. Chapter 3 presents the implementation of bonded contact model in LS-Dyna and describes the parameters required for the formation of a bond. With the LS-Dyna in-built particle generation module, the particle packing density is studied to optimize the particle size required for subject modeling. Parameters for bond initialization and bond failure are further discussed. Chapter 4 presents a parametric study to understand the influence of input parameters of bonded contact model on the bulk response material response. The DEM models used are two-particle and three-particle models and various parameters are varied to study the response of these systems. Chapter 5 describes the model geometry, loading configuration and boundary conditions. It also presents the calibrated model with its values, using the results from parametric study from Chapter 4. Chapter 6 discusses the bulk mechanical properties such as strain at failure, Poisson's ratio and volumetric strains for each sample with varying particle size. The effect of particle size on these quantitis is also presented. Overall damage behavior and failure patterns on the samples are investigated. Chapter 7 summarizes the overall conclusions that can be drawn from the present study and recommendations for future work are made.

CHAPTER 2: THE DISCRETE ELEMENT METHOD

2.1 General Background on DEM

In the Discrete Element Method, the body of interest is discretized into a collection of discrete, rigid particles. These particles contain all the mass of the system and interact with each other at their contacts, the particles may overlap and the resulting interaction force is directly proportional to the magnitude of overlap. A contact is necessary for particles to interact in the case of non-bonded particles however not required in the case of bonded particles. In the case of modeling cementitious materials such as concrete, a contact can still exist between two particles even if there is no substantial overlap between them. The overlap of particles represents the deformation of surfaces that occurs when grains come into contact as in the physical material. It is assumed that this overlap area is relatively small compared to the dimensions of the corresponding particle. DEM provides a three-stage calculation cycle which calculates the dynamic interaction of each element in contact. The three stages are; contact detection, calculation of interaction forces and numerical time integration. The process flow chart for overall working of DEM is shown in Figure 3. Once the contacts are determined, the internal forces resulting from particle interactions are determined using the force-displacement laws that are dictated by the choice of the contact model. Newton's second law of motion is used to calculate acceleration for

each element based on the summation of internal and external forces. These accelerations are then time integrated to calculate new positions of each element, with an advancement in time step. The new positions now corresponds to new contacts. This cycle continues until a specified amount of end time is reached.

This study focuses on the bonded particle models, since bonded contact models are the most commonly used models that are capable of representing the bonding between particles in actual material as in cementitious materials like concrete. Models used to mimic the behavior of cementitious materials are required to have a contact law that deals with non-bonded as well as bonded contacts. A non-bonded contact later may arise either due to bond breakage or particles coming in contact after the bond initializing process. The simulations in the present work are carried out using the DEM software LS-Dyna (Livermore Software Technology Corporation). The bonded particle model in LS-Dyna is based on the work by Potyondy and Cundall [26]. Particles with non-bonded contact are simulated with the Hertz-Mindlin contact model discussed by Cundall and Strack [9]. Both the above contact models are discussed as follows.

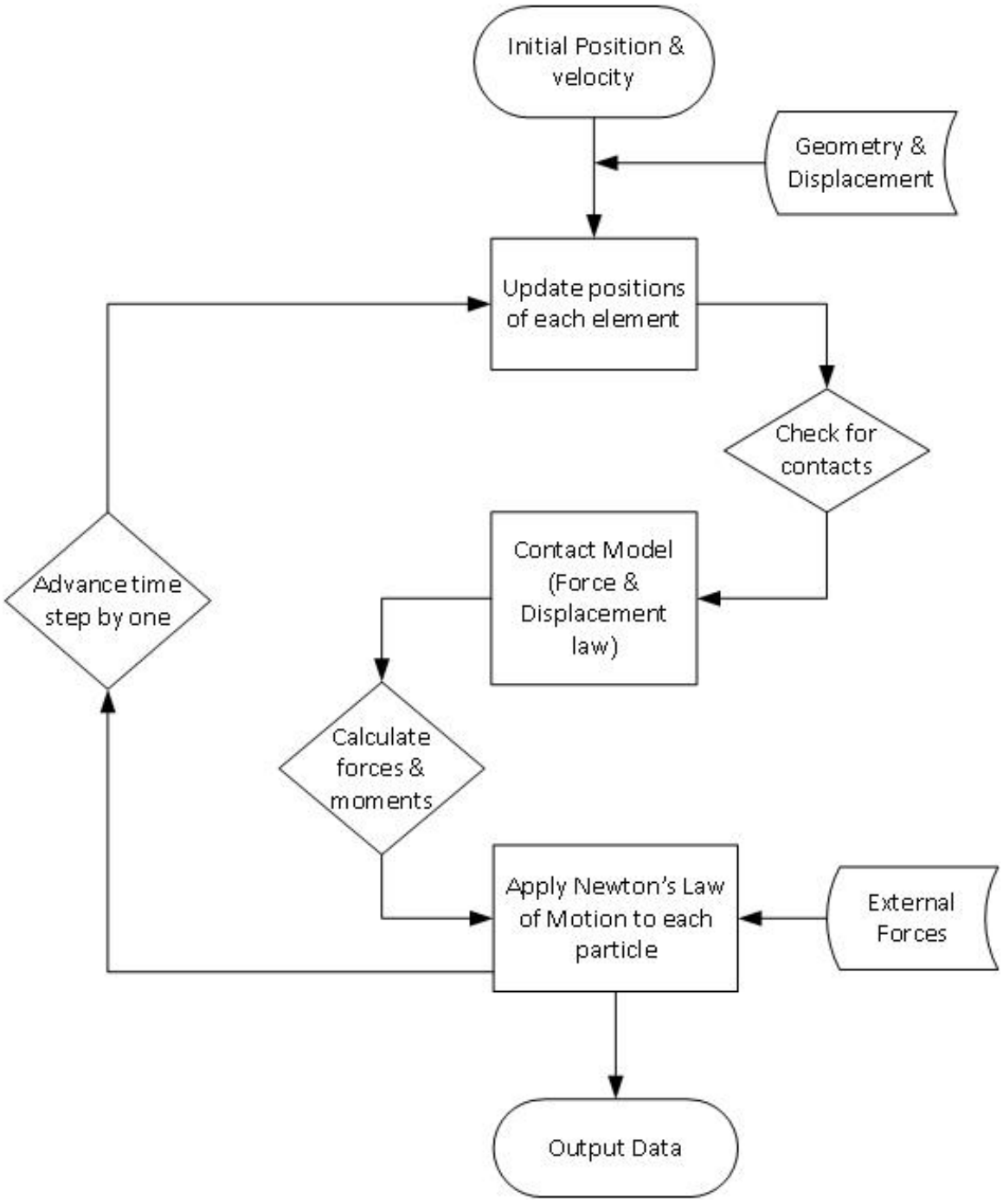

Figure 3: A Schematic of a DEM calculation cycle. (Adapted from [5])

2.2 The Hertz-Mindlin Contact Model

The Hertz-Mindlin Contact Model (HMCM) is used to describe the force-displacement relationship at non-bonded contacts; non-bonded contacts occur either through the breakage of bonds or from two particles coming into contact for the first time. As shown in Figure 4, the HMCM assumes spring-dashpot systems in tangential and normal directions and takes into account the full 3D interaction of two elements. Hertzian-type contacts are used for normal forces, the effects of tangential forces are considered according to the models developed by Mindlin and Deresiewicz; see Nayak ([20],[22]).

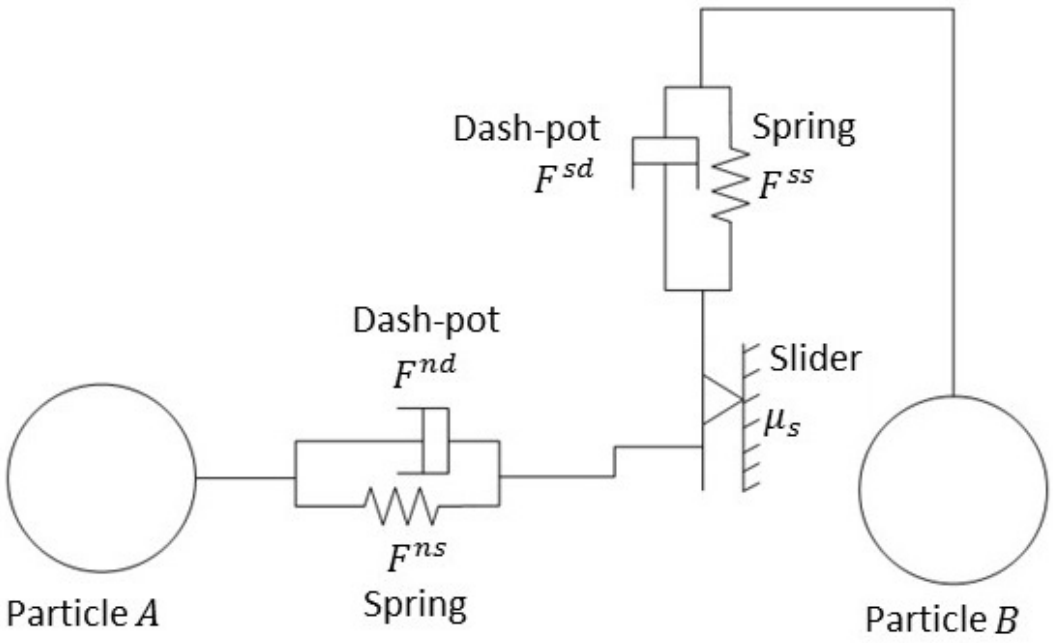

Figure 4: A two particle spring dash-pot configuration.

The normal force F^n and tangential force F^s at non-bonded contacts are calculated as the sum of their respective spring forces, F^{ns} or F^{ss} and damping forces F^{nd} or

F^{sd} so that:

$$F^n = F^{ns} + F^{nd} \tag{1}$$

and

$$F^s = F^{ss} + F^{sd} \tag{2}$$

The normal and tangential forces due to the spring (denoted by F^{ns} and F^{ss}) and due to the damper (denoted by F^{nd} and F^{sd}) are given by:

$$F^{ns} = \frac{4}{3} E_c \sqrt{R} U^{n1.5}, \tag{3}$$

$$F^{nd} = -2\sqrt{\frac{5}{6}} \xi_d \sqrt{K_n \bar{m}} V_n, \tag{4}$$

$$F^{ss} = -K_s U^s, \tag{5}$$

and

$$F^{sd} = -2\sqrt{\frac{5}{6}} \xi_d \sqrt{K_s \bar{m}} V_s \tag{6}$$

respectively. Here, E_c is the equivalent Young's modulus of the two particles, R is the equivalent radius, U^n and U^s are the normal and tangential overlap respectively, ξ_d is the damping ratio related to the coefficient of restitution e, $\bar{m}$ is the equivalent mass, V_n and V_s are the normal and tangential components of relative velocity. The tangential force is limited by Coulomb Friction, i.e.,

$$F_s \leq \mu_s F^n \tag{7}$$

with μ_s being the coefficient of static friction.

The normal stiffness k_n and tangential stiffness k_s are:

$$k_n = 2E_c\sqrt{RU^n}, \tag{8}$$

$$k_s = 8\bar{G}\sqrt{RU^s}, \tag{9}$$

and

$$\frac{1}{\bar{G}} = \frac{1-{\nu_A}^2}{G_A} + \frac{1-{\nu_B}^2}{G_B}. \tag{10}$$

Here, $\bar{G}$ is the equivalent shear modulus, ν_A and ν_B are the Poisson's ratio of the particles A and B. Clearly, this contact model provides a non-linear relationship between the force and overlap.

2.3 Bonded Particle Model in DEM

The mechanical behavior of a cementitious material such as concrete is governed by the formation, growth and the propagation of cracks through the interaction of micro-cracks. Microscopic observations of cementitious material reveal comprehensive information about initial defects and load-induced cracks, such as length, density, aspect ratio and orientation([24],[14]). Experimental observations reveal that compression-induced cracks are the ones that proliferate at the initial faults, such as grain boundaries or crack-like, low-aspect-ratio cavities and voids, and that all compression-induced cracks are almost parallel to the direction of the maximum compression. Compression-induced tensile crack has a substantial importance in produc-

ing extensile crack growth[16].

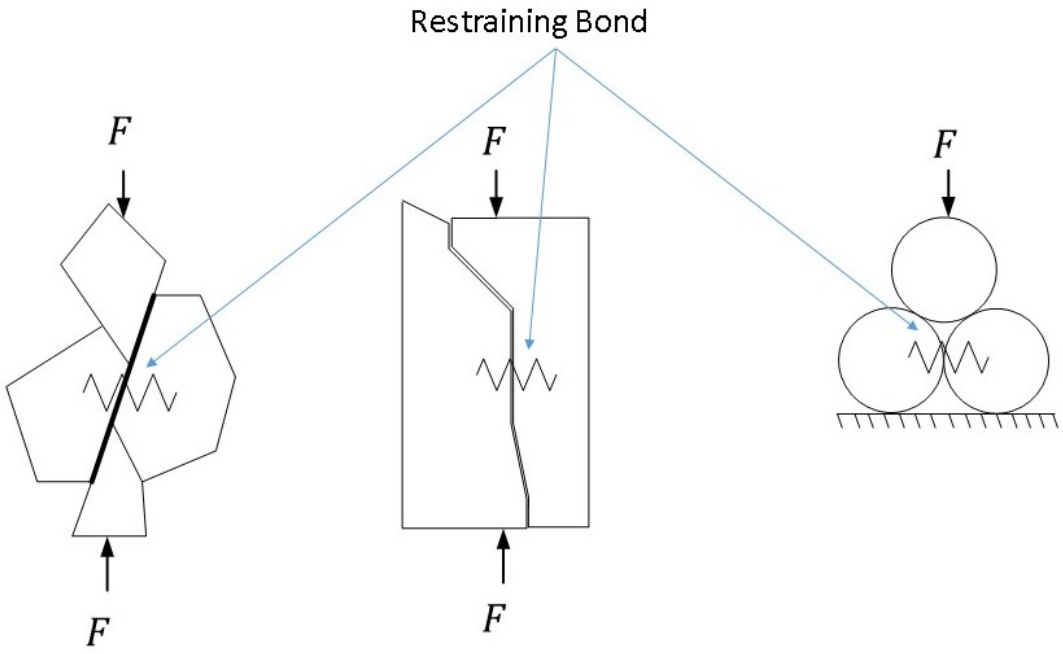

Figure 5: A representation of compression-induced tensile cracking and its idealization as bonded assembly of spherical particles. (Adapted from [26])

A mechanism for the formation of compression-induced tensile cracks is shown in Fig 5, in which a group of elements are forced apart by an axial load, causing the restraining bond to experience tension. With the formation and growth of micro-cracks, the subsequent interaction of these cracks is necessary to produce local failure such as axial splitting or element separation during unconfined or confined compression tests. A concrete model, intending to reproduce these phenomena, must allow the micro-cracks to interact with one another[26].

The contact model used in the software package LS-Dyna for bonded particles is the BPM as proposed by Potyondy and Cundall [26]. This model approximates the grains of granular material by spherical spheres and represents the cemented bonds by beam elements which are connected to centers of two particles as shown in Figure

7.

The BPM simulates the mechanical behavior of a collection of rigid spherical particles that are bonded together at their contact points. The rigid particles interact at their bonds that possess finite normal and shear stiffnesses and finite strengths in both normal and shear directions. The BPM model with a bond between two particles known as a parallel-bond can be envisioned as an elastic beam connecting the two bonded particles with its ends at the particle centers. It is this virtual elastic beam at each bonded contact that accommodates tension, bending, shearing and twisting between bonded particles (see Figure 6).

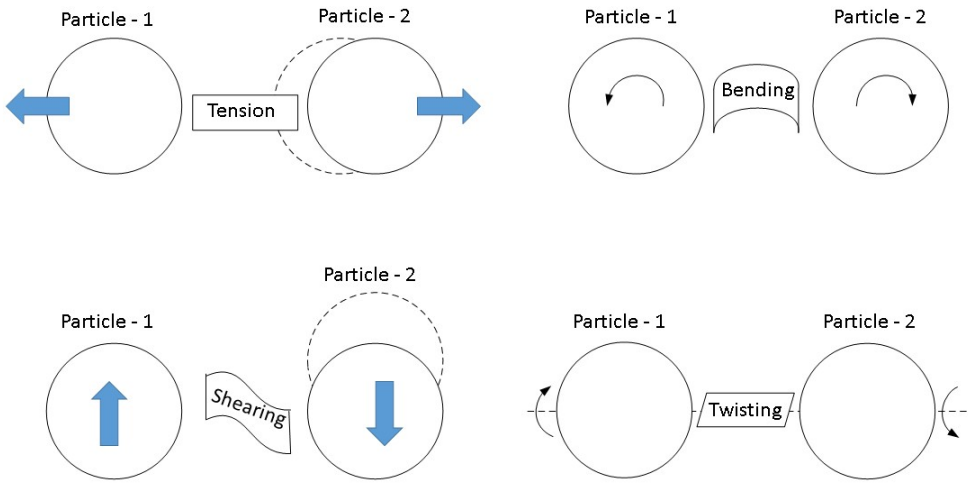

Figure 6: A representation of a parallel-bond with BPM model that can accommodate various forces and moments between two bonded particle. (Adapted from [15]).

The mechanical behavior of the bonded-particle system is described by the movement of each particle and the force and moment acting at each contact. Newton's laws of motion provide the fundamental relations between particle motion and the

resultant forces and moments causing that motion. The main assumptions in the BPM models are as follows [26]:

- The particles are circular (2D) or spherical (3D) rigid bodies with a finite mass.
- The particles move independently of one another and can both translate and rotate.
- The particles interact only at contacts; because the particles are circular or spherical, a contact is comprised of exactly two particles.
- The particles are allowed to overlap one another, and all overlaps are small in relation to particle size such that contacts occur over a small region (i.e., at a point).
- Bonds of finite stiffness can exist at contacts, and these bonds carry load and can break. The particles at a bonded contact need not overlap.
- Generalized force-displacement laws at each contact relate relative particle motion to forces and moments at the contact.

The cement-based portion of the force-displacement behavior at each cemented contact is described by the following five parameters that define a parallel-bond (see Fig. 7): normal and shear stiffnesses per unit area, $\bar{k}^n$, $\bar{k}^s$; tensile and shear strengths, $\bar{\sigma}_c$ $\bar{\tau}_c$; and bond-radius multiplier, λ, such that the parallel-bond radius is given by:

$$\bar{R} = \bar{\lambda}\, min\left(R^A, R^B\right) \tag{11}$$

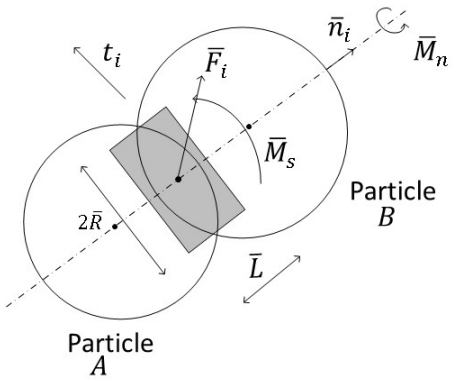

Figure 7: Force displacement behaviour of bonded particles.

with R^A and R^B being the particle radii. A parallel-bond can be idealized as a set of elastic springs uniformly distributed over a rectangular cross-section of the beam lying on the contact plane and centered at the contact point. These springs behave as a beam whose length $\bar{L}$, approximates the mechanical behavior of a joint. The total force and moment carried by the parallel-bond are denoted by $\bar{F}_i$ and $\bar{M}_i$, respectively, which represent the action of the bond on particle B. The force and moment vectors can be resolved into normal and shear components with respect to the contact plane as:

$$\bar{F}_i = \bar{F}^n n_i + \bar{F}^s t_i \tag{12}$$

and

$$\bar{M}_i = \bar{M}^n n_i + \bar{M}^s t_i \tag{13}$$

where $\bar{F}_n$, $\bar{F}_s$ and $\bar{M}_n$, $\bar{M}_s$ denote the axial- and shear-directed forces and moments, respectively, and n_i and t_i are the unit vectors that define the contact plane. When the parallel-bond is formed, $\bar{F}_i$ and $\bar{M}_i$ are initialized to zero. Each subsequent relative displacement and rotation increment produces an increment of elastic force and moment that is added to the current values. The increments of elastic force and moment are given by:

$$\Delta \bar{F}^n = \bar{k}^n \, A \, \Delta U^n, \tag{14}$$

$$\Delta \bar{F}^s = -\bar{k}^s \, A \, \Delta U^s, \tag{15}$$

$$\Delta \bar{M}^n = -\bar{k}^s \, J \, \Delta \theta^n, \tag{16}$$

and

$$\Delta \bar{M}^s = -\bar{k}^n \, I \, \Delta \theta^s \tag{17}$$

where, A,I and J are the area, moment of inertia and polar moment of the parallel-bond cross-section, respectively. These quantities are given by:

$$A = \pi \bar{R}^2, \tag{18}$$

$$I = \frac{1}{4} \pi \bar{R}^2, \tag{19}$$

and

$$J = \frac{1}{2}\pi \bar{R}^2. \tag{20}$$

The maximum tensile and shear stresses acting on the parallel-bond periphery are calculated from beam theory to be:

$$\bar{\sigma}^{max} = \frac{-\bar{F}^n}{A} + \frac{\left|\bar{M}^s\right| \bar{R}}{I} \tag{21}$$

and

$$\bar{\tau}^{max} = \frac{|\bar{F}^s|}{A} + \frac{\left|\bar{M}^n\right| \bar{R}}{J}. \tag{22}$$

If the maximum tensile stress exceeds the tensile strength $[\bar{\sigma}^{max} \geq \bar{\sigma}_c]$ or the maximum shear stress exceeds the shear strength $[\bar{\tau}^{max} \geq \bar{\tau}_c]$, then the bond is considered broken and removed from the model along with its accompanying force, moment and stiffness.

CHAPTER 3: DEM IN LS-DYNA

3.1 Contact model

The interaction of particles in DEM is through contact forces or forces due to bonding. These forces and interaction in particles determine the overall behavior of the material. The interaction between particles require an appropriate contact law to be defined (as discussed in Chapter 2). The contact laws are the key components to formulate the microscopic behavior of the material model. For modeling cementitious materials such as concrete, bonds are assumed to exist between particles. These give rise to bond forces that are similar to the internal forces in a continuum body. The bonds are virtual and have no physical mass associated with it. Particle interactions can be classified as non-bonded contact models and bonded-particle models. As mentioned in Chapter 2, in the present work, it is the bonded-particle models that are used to model compression of concrete. The DEM capabilities of the commercial finite element software LS-Dyna is used for this purpose. For the study of cementitious material like concrete, LS-Dyna uses two contact models each for non-bonded and bonded contacts. The Hertz-Mindlin (HMCM) and BPM contact models are used for non-bonded and bonded contacts respectively. Non-bonded contacts may arise due to the breakage of bonds and when two particles come into contact after the bond initialization procedure. The implementation of BPM contact model augments the

overall DEM process with a bond initialization procedure where bonds are created using a proximity criteria. The flow chart in Figure 8 summaries the integration of BPM model into the explicit time-step cycle employed in the working of DEM.

As stated in Chapter 1, particles can be generated through different techniques. However, each particle generation technique creates a different initial packing arrangement of particles. This study (which uses LS-Dyna) uses a geometry-based approach to generate particles in the domain specified by the user. The initial packing arrangement and the packing density chiefly defines the geometric properties and the total number of bonds. In the following, the packing density and the distribution of particle sizes on it are presented.

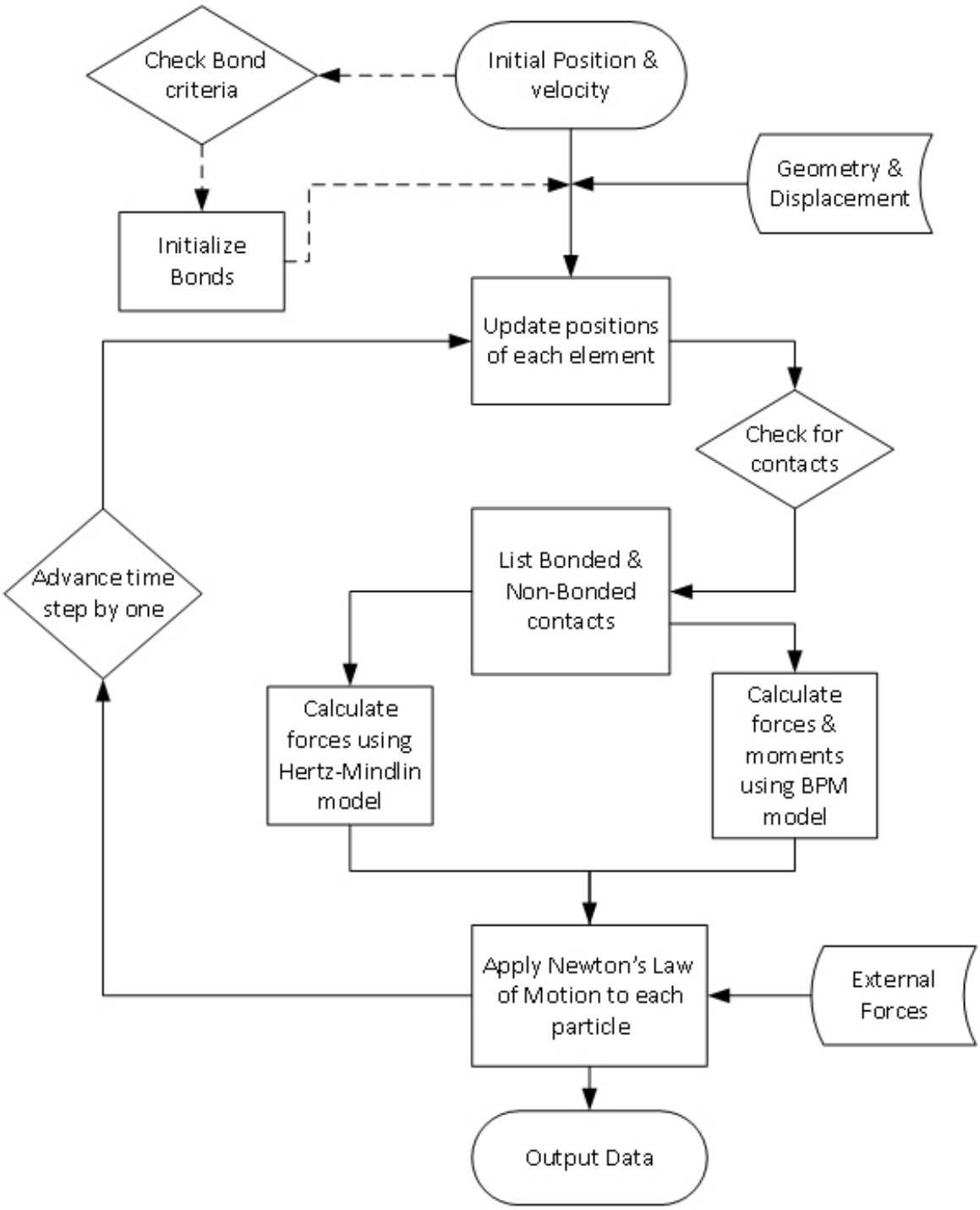

Figure 8: Flowchart representing the implementation of BPM model into the calculation cycle of DEM. (Adapted from [5])

3.2 Element generation and packing

Generation of a suitable initial configuration of particles is a critical step in every DEM simulation. When conducting any DEM modeling, it is crucial that the generated particle packing is representative of the volume of the material that is to studied. The microscopic grain structures of cementitious materials are highly inhomogeneous, often including voids or inclusions which provide natural weaknesses. Due to the wide range in grain sizes, especially in concrete where fine sand grains can be much smaller than the coarse aggregates, DEM models do not essentially model every individual grain. Assumptions have to be made, and larger elements are often used to represent a portion of the sample. The elements at the mesoscopic scale incorporate properties of the microstructure and directly affect the properties of the bulk solids. Since particle packing directly affects the properties of the macrostructure, the discretization should be primarily taken into account when considering the calibration of the model. As mentioned in Chapter 1,LS-Dyna uses algorithms that are purely based on the geometry of the domain. LS-Dyna uses advancing front approach [11] to generate particles in a closed domain.

Numerical experiments were carried out to calculate packing densities of various sizes of particles for the optimal selection of the range of size and distribution of particles for the problems considered in this thesis. Packing density is defined as:

$$Packing\ density(\%) = \frac{volume\ of\ solids}{volume\ of\ geometry} \times 100. \tag{23}$$

Numerical tests were performed for a mono-disperse particle distribution on a sam-

ple cylindrical domain with the parameters in Table 1. Various particle sizes were tested ranging from 0.05 to 2.5 to calculate packing densities as given in Table 2.

Table 1: Cylinder parameters of test sample used to examine packing densities.

Height (mm)	Radius (mm)	Total volume (mm^3)
10	5	785.398

Table 2: Calculated packing densities for different particle sizes.

Particle size (mm)	Volume of each particle (mm^3)	Total no. of particles	Total particle volume (mm^3)	Packing density (%)
2.5	65.45	3	196.34	25
2	33.51	6	201.06	25.6
1.5	14.13	17	240.33	30.06
1	4.18	72	301.59	38.4
0.5	5.23E-1	685	358.66	45.63
0.25	6.544E-2	6063	396.82	50.5
0.1	4.188E-3	100216	419.78	53.4
0.05	5.23E-4	815821	427.162	54.38

The Figure 9 shows the relation between particle size and particle densities. Based on the trials performed, it is clear that the advancing front approach algorithm used by LS-Dyna has a highest packing density in the range of 55% to 60% without further rearrangement. It can be concluded that a particle size 40 times smaller than the minimum dimension of the domain is sufficient to produce packing densities above 52%. Any decrease in the particle radius does not increase the packing density substantially, however this increases the number of particles and total simulation time by a large amount. Hence, in the present work, particle density densities in the range of 50%-55% are considered to be desirable.

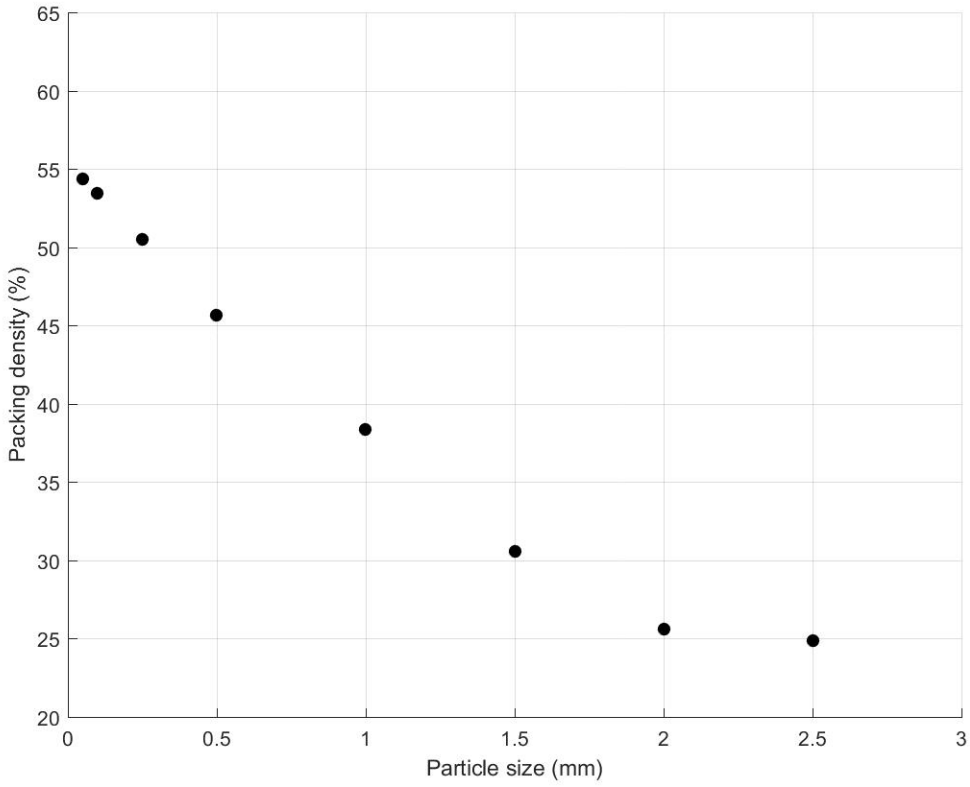

Figure 9: Effect of particle size on packing density.

3.3 Initialization of bonds

Bond models designed to simulate the behavior of cementitious materials such as concrete differ from other models in the way the cement joints between grains are captured. In BPM method used by LS-Dyna, this mechanism is represented by a bonded contact which is capable of resisting the separation of the particles it connects. An initialization procedure is required to determine which elements are considered bonded and which are not. For most bond models, a criterion exists which must be met for two particles to be considered bonded; the BPM method in LS-Dyna uses proximity parameter as a criterion for bonding of two elements. The user defined

card *DEFINE_DE_BOND initializes the bond and defines all the required variables required for a successful bond generation. Table 3 shows the variables used in the user defined card.

Table 3: Bond parameter card *DEFINE_DE_BOND in LS-Dyna.

PBN	PBS	PBN_S	PBS_S	SFA	ALPHA	MAXGAP
G_b	$\bar{k}^s/\bar{k}^n$	$\bar{\sigma}_c$	$\bar{\tau}_c$	λ	α	$\bar{X}$

G_b is the parallel-bond modulus

where

$$G_b = \bar{k}^n L \tag{24}$$

and $L = R^A + R^B$. In addition, $\bar{k}^s/\bar{k}^n$ is the parallel-bond stiffness ratio, $\bar{\sigma}_c$ is the parallel-bond normal strength, $\bar{\tau}_c$ is the parallel-bond shear strength, λ is the bond radius multiplier, α is the numerical damping, and $\bar{X}$ is the maximum gap between two bonded particles.

The parameter $\bar{X}$ defines the extension for a contact search of a neighboring particle that has to be bonded. Thus, any two particles which are not in physical contact with each other may still be bonded together. If the parameter $\bar{X}$ is reduced, the total number of bonds will reduce and thus the material being represented will behave more granular in nature. The parameter $\bar{X}$ can be reduced to zero, in this case, the particles would have to be in direct contact with each other to form a bond between them.

The contact model that describes the force-displacement law for a bonded particle

requires the geometric dimensions of the bond to be defined. For a spherical particle, the bond is assumed to be cylindrical in shape with a uniform cross-section. The length of the bond is the distance between centers of two particles that are bonded. For a uniform cylinder, the radius $\bar{R}$ is determined by Equation 11, where λ, the bond radius multiplier acts as a scaling factor to vary its magnitude.

3.4 Bond failure criteria

For a cementitious material like concrete, under loading, the material will have a microscopic failure when the compression induced tensile loading on two cemented elements exceeds the cement strength. This is represented in DEM particles as the the failure of bonded particles when the loading exceeds the bond strength. The material will undergo total failure when enough bonds are broken. The phenomenon of bonds breaking at any location when bonding strength exceeds give the advantage over Finite Element Method (FEM) in terms of crack formation and propagation.

The failure of bonds which represents the fracture in a cementitious material requires a method through which the bonds between particles can break. This mode of bond failure is a predefined failure criterion. For a BPM model discussed in this study, bond failure criteria are based on limits of forces and are given by the Equation 21 and 22.

CHAPTER 4: PARAMETRIC STUDY: INFLUENCE OF INPUT PARAMETERS

In this chapter, a parametric study examining the influence of various parameters of the BPM contact model on the DEM behavior is presented. Since many parameters govern the BPM contact model with each parameter contributing independently to the overall material behavior, understanding the influence of these parameters while keeping other parameters the same is critical for the accurate calibration of a model. This study is carried out in the context of concrete. Hence the parameters for bonded contact will have the most influence over non-bonded contact. To better understand a specific parameter and its direct impact on material behavior, simpler models consisting of two-particle and three-particle models are used initially. Four important parameters in the bonded contact model are of interest. In the following, these are discussed in detail.

4.1 Influence of parallel-bond modulus

A two-particle model was used to study the effect of this parameter. Figure 10 shows a two particle configuration in which particle-1 is fixed at its center, and particle-2 is axially loaded with a known force. A diameter of 1 mm is used for both the particles. The particles do not have any overlap and are just in contact with each other. The parallel-bond modulus G_b was varied from 100 GPa to 200 GPa keeping all other bond parameters same. Table 4 gives the values for bonded contact

parameters used in this parametric study.

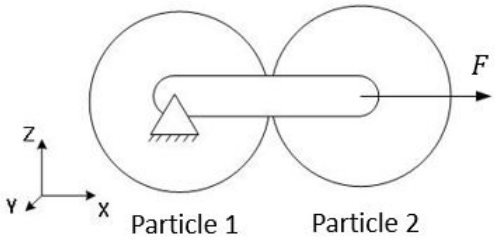

Figure 10: A two particle model subject to pure axial loading.

Table 4: Bonded contact parameters used to examine the influence of parallel-bond modulus.

G_b (GPa)	$\bar{k}^s/\bar{k}^n$	$\bar{\sigma}_c$ (GPa)	$\bar{\tau}_c$ (GPa)	λ	α	$\bar{X}$ (mm)
100 - 200	0.5	1.0	1.0	1.0	0.2	0.1

For each known force, the axial displacement of particle-2 is recorded for various values of G_b . Table 5 shows the axial displacements obtained for each parallel-bond modulus. Figure 11 shows the force-displacement curves.

Table 5: X-axial displacements of particle-2 with varying parallel-bond modulus.

G_b	Axial displacement of particle-2 (mm)			
	F =1.5 KN	F =2.0 KN	F =2.5 KN	F =3.0 KN
100	0.00955	0.0127	0.0159	0.0191
125	0.00764	0.0102	0.0127	0.0153
150	0.00637	0.00849	0.0106	0.0127
175	0.00546	0.00728	0.00909	0.0109
200	0.00477	0.00637	0.00796	0.00955

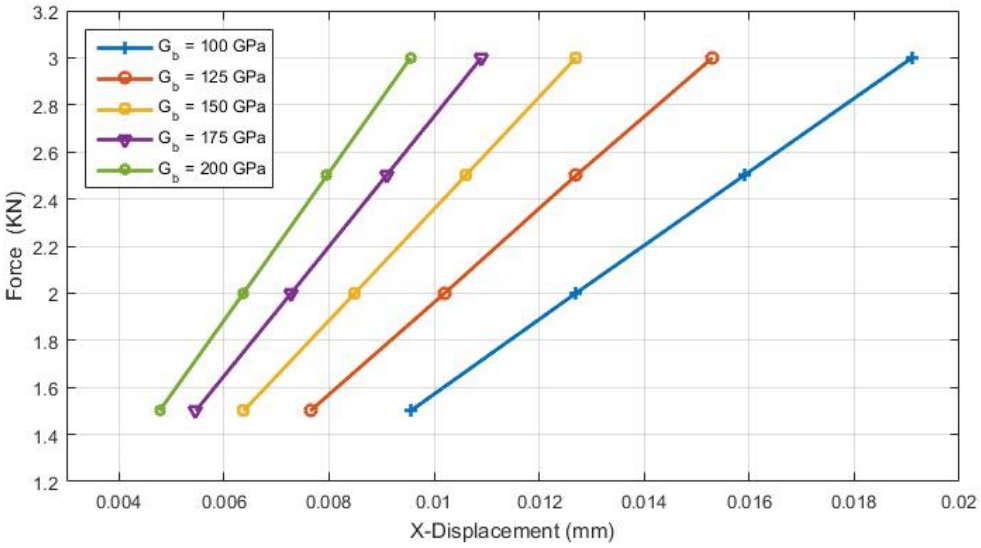

Figure 11: Force-displacements curves for varying parallel-bond modulus.

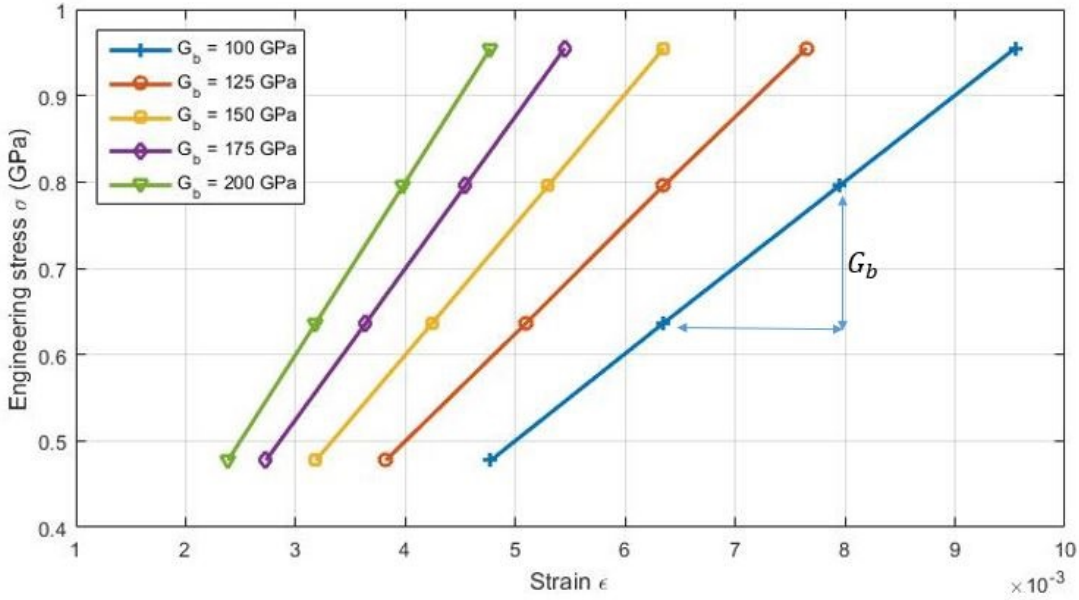

Figure 12: Engineering stress-strain curves for varying parallel-bond modulus.

The bond's virtual beam dimensions can be calculated using Equation 11. With the known cross-section area and length of beam, an engineering stress-strain curve is plotted (see Figure 12). As the parallel-bond stiffness increases, the strain for a

given stress decreases. Furthermore, it can be seen from Figure 12 that the slope of each stress-strain curve is equal to its magnitude of parallel-bond modulus. This is analogous to the Young's modulus of an elastic material.

4.2 Influence of parallel-bond stiffness ratio

A parallel-bond stiffness ratio is defined as the ratio of parallel-bond shear stiffness to parallel-bond normal stiffness. This gives the magnitude for parallel-bond shear stiffness with respect to parallel-bond normal stiffness. To understand the influence of parallel-bond stiffness ratio on a DEM system, a three-particle model was used. Figure 13 shows a model of three particles, where the bottom particles are placed over a rigid plate and their motion is constrained in Y-direction. The top particle is given a displacement loading in Z-direction through a top rigid plate. Particles are just in contact with each other without any overlap. The centers of all three particles are co-planar.

The parallel-bond stiffness ratio was varied from 0.5 to 0.9. For each parallel-bond stiffness ratio, Z-displacement of the top particle and lateral displacements for bottom particles were recorded at 50% of maximum-bond breakage strength. With the known displacements of particles in axial and lateral directions, axial and lateral strains are calculated as follows:

$$\epsilon_z = \frac{\delta z}{z_0} \tag{25}$$

and

$$\epsilon_x = \frac{\delta x}{x_0} \tag{26}$$

where ϵ_z is the axial strain, ϵ_x is the lateral strain, δz, δx are the axial and lateral displacements of top and bottom particles respectively. The subscript 0 represents the initial values.

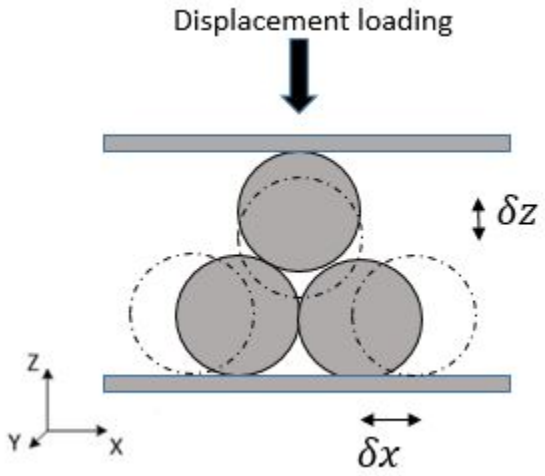

Figure 13: Engineering stress-strain curves for varying parallel-bond modulus.

With axial and lateral strains, a ratio of these strains, here proposed as *particle strain ratio* (P_{sr}), is calculated as:

$$P_{sr} = \frac{\epsilon_x}{\epsilon_z}. \tag{27}$$

Table 6 gives the values for bonded contact parameters used in this parametric study. Table 7 gives the values for particle strain ratio for each parallel-bond stiffness ratio.

Table 6: Bonded contact parameters used to examine the influence of parallel-bond stiffness ratio.

G_b (GPa)	$\bar{k}^s/\bar{k}^n$	$\bar{\sigma}_c$ (GPa)	$\bar{\tau}_c$ (GPa)	λ	α	$\bar{X}$ (mm)	Particle radius (mm)
150	0.5-0.9	1.0	1.0	1.0	0.2	0.1	1.0

Table 7: Particle strain ratio with varying parallel-bond stiffness ratio.

$\bar{k}^s/\bar{k}^n$	ϵ_x	ϵ_z	P_{sr}
0.5	8.34E-5	2.73E-4	0.30
0.6	1.20E-4	2.84E-4	0.42
0.7	1.64E-4	2.93E-4	0.55
0.8	2.14E-4	3.07E-4	0.69
0.9	3.01E-4	3.62E-4	0.82

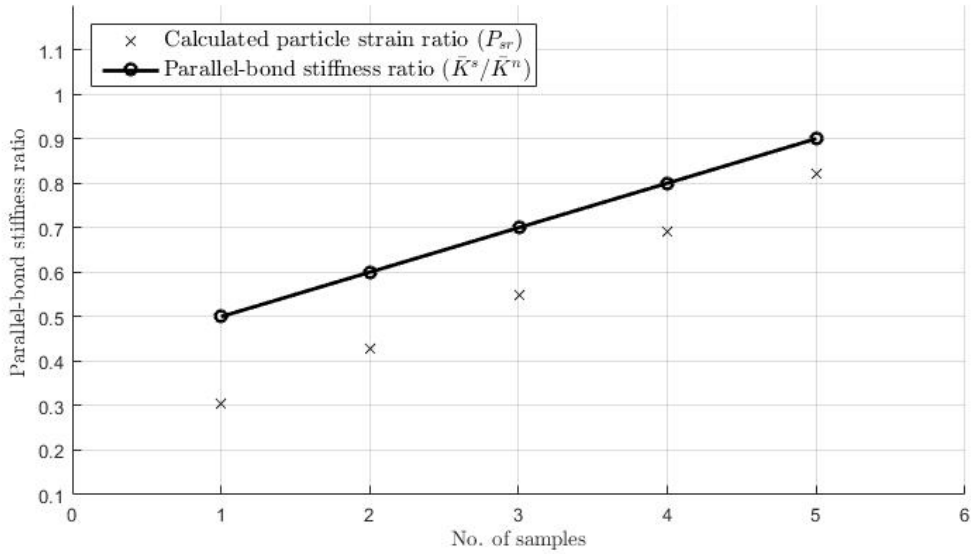

Figure 14: Particle strain ratio for varying parallel-bond stiffness ratios.

Figure 14 shows that as the parallel-bond stiffness ratio ($\bar{k}^s/\bar{k}^n$) increases, the particle strain ratio (P_{sr}) also increases in the same proportion. The value of particle stiffness ratio also remains close to the specified parallel-bond stiffness ratio. The bulk behaviour of a model in axial and lateral strain is largely dependent on the value specified as parallel-bond stiffness ratio. With this parametric study it can be concluded that a parallel-bond stiffness ratio is analogous to Poisson's ratio in an elastic body. However, it should be noted that a more realistic model with a large number of particles is needed to draw a direct comparison between P_{sr} and the

Poisson's ratio of a material.

4.3 Influence of parallel-bond normal strength

Parallel-bond normal strength $\bar{\sigma}_c$ is defined as the maximum stress in normal direction that the bond can withstand before failing. For a bonded contact model, this value is specified through the failure criterion as given in Equation 21. Equation 21 shows that normal force acting on the bond and the critical stress due to the applied force are linearly proportional. Thus, any increase or decrease in the parallel-bond normal strength will limit the critical stress in a bond linearly. The linear relation between parallel-bond normal strength and the maximum stress at failure in a bond can be verified with a two-particle model as shown in Figure 10. A normal force is applied to the bond for various values of the parallel-bond normal strength parameter. The maximum forces at failure are recorded for various values of the parallel-bond normal strength. With known dimensions of the virtual beam-bond, stresses are calculated at bond failure, and a graph is plot for maximum stress vs. parallel-bond normal strength as shown in Figure 15. In this parametric study, the maximum stress at failure is calculated from:

$$\sigma_{max} = \frac{F_{max}}{A} \tag{28}$$

where A is the area of cross-section of the virtual beam bond. Table 8 gives the contact parameters used to examine the influence of parallel-bond normal strength on DEM behavior.

Table 8: Bonded contact parameters used to examine the influence of parallel-bond normal strength.

G_b (GPa)	$\bar{k}^s/\bar{k}^n$	$\bar{\sigma}_c$ (GPa)	$\bar{\tau}_c$ (GPa)	λ	α	$\bar{X}$ (mm)	Particle radius (mm)
150	0.5	0.25-1.25	1.0	1.0	0.2	0.1	1.0

Table 9: Maximum stress at failure with varying parallel-bond normal strength.

$\bar{\sigma}_c$ (GPa)	F_{max} (KN)	σ_{max} (MPa)
0.25	0.9	286.47
0.5	1.6	509.29
0.75	2.4	763.94
1.0	3.20	1018.59
1.25	3.95	1257.32

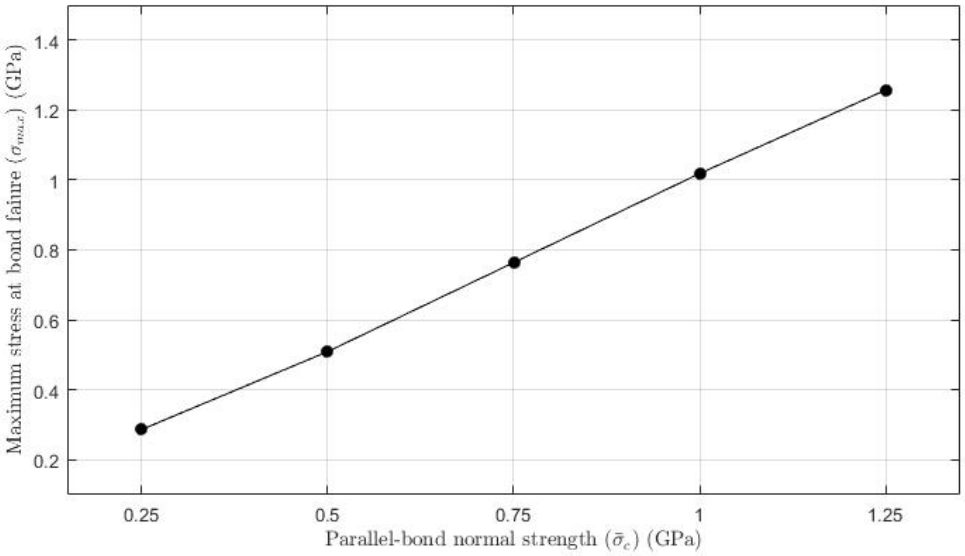

Figure 15: Influence of parallel-bond normal strength on maximum stress at bond failure.

4.4 Influence of parallel-bond shear strength

Similar to parallel-bond normal strength, parallel-bond shear strength is also defined as the maximum stress in shear, the bond can withstand before failing. Equation 22 gives the failure criterion of a bond in shear. Similar to parallel-bond normal strength, a linear relation exists between parallel-bond shear strength and the maximum stress in shear at failure in a bond.

4.5 Summary of bonded contact parameters

For a concrete material under compressive loading, as the load increases, more and more bonds fail as the contact forces continue to exceed the bond-failure loads. Once a substantial number of bonds are broken, and the material reaches post failure loading, the non-bonded contact parameters begin to influence more over the bonded contacts. However, in this thesis which limits its research up to the material failure, the bonded contact parameters play a major role in the characterization of material behavior. As studied from the parametric study for parallel-bond modulus, the bond modulus has a direct effect on the stiffness on each bond and hence on the overall bulk stiffness. This also affects the bulk strain response. For example, if the stiffness of the bond is decreased, deformation increases for a given force in each bond, and thus resulting in an increased strain at failure. Parallel-bond stiffness ratio directly affects the strain in the bulk response but does not affect the stiffness of the material. It also defines the distribution of normal stiffness over shear stiffness in the material model.

In summary, it can be concluded that, while keeping the particle size same, parallel-

bond modulus and parallel-bond stiffness ratio affect the stiffness characteristics of each bond and the parallel-bond normal and shear strength characterize the normal and shear limits for each bond respectively. Simpler models with a very few number of particles can be used very effectively to study the effect of these parameters on the overall system response.

CHAPTER 5: MODELING OF A CONCRETE CYLINDER

This chapter describes the discrete element approach to modeling the response of a 3D concrete cylinder to uniaxial compression. Guided by the study of the two-particle and three-particle systems discussed in Chapter 4, a set of parameters is derived after calibration simulations performed. The predictive capabilities of these calibrated parameters are simulated using four cylindrical samples of varying particle size under uniaxial compression. For a loading configuration and specimen geometry, the effort is to mimic a physical test of concrete cylinder under uniaxial test. The cylinder geometry, bonded and non-bonded parameters and FEM-DEM contact parameters are discussed in details in the following.

All simulations were carried out with LS-Dyna SMP, double precision, R8.0.0 and were run on *Copperhead*, a Redhat Linux-based, high performance computing (HPC) cluster at UNC Charlotte, with dual Intel Xeon 3.2 GHz 8-core processors and 128 Gb RAM.

5.1 Geometry

Figure 16 shows a cylinder geometry and the DEM model. LS-Dyna requires an initial shell volume for the generation of DEM particles. As discussed in the introduction part of Chapter 1, the advance front approaching method for generating particles was used using the built-in sphere packing engine from LS-PrePost. This

gives the option to the user to create particles with user defined radii. All particles once generated are recorded for their respective coordinates in the keycard *ELEMENT_DISCRETE_SPHERE_VOLUME. To simulate uni-axial loading configuration, the DEM particles are placed between two FEM rigid body plates. The plates are 80 mm × 80 mm and 5 mm thick each.

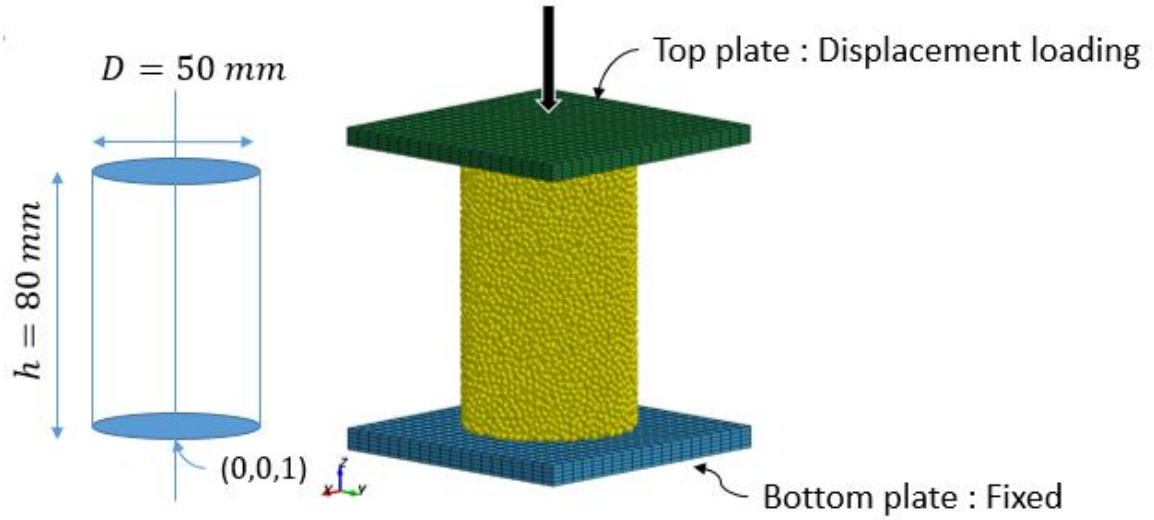

Figure 16: Geometry of DEM cylinder specimen and loading configuration.

5.2 Boundary conditions

The loading configuration of DEM in uni-axial loading is achieved through displacement loading at top plate using the keycard *BOUNDARY_PRESCRIBED_MOTION_RIGID. The bottom plate is constrained in all 3 DOFs. Top plate is constrained in X and Y displacements and displacement is given in Z -axis. To mimic quasi-static loading conditions, the loading rate is taken to be 0.03 mm/ms. The total kinetic energy of the system remains within 1.5E-4 KN-mm until failure and particle separation. Both the plates are considered rigid

and the material parameters are given in Table 10. Although these parameters do not affect the material behavior and resultant force acting on FEM-DEM contact, these parameters are required for particle-wall non-bonded contact model. DEM particles are free in all 6 DOFs.

Table 10: Material parameters for rigid plates.

Parameter	Description	Value
ρ	density (kg/mm^3)	7.83E-6
E	Modulus of elasticity (GPa)	200
ν	Poisson's ratio	0.3

5.3 FEM-DEM contact

The 3D model requires a contact to be defined between DEM elements and FEM rigid plates. This contact is formulated using the key-card *CONTACT_AUTOMATIC_NODES_TO_SURFACE. The contact uses static friction coefficient (FS) between DEM particles and plates and viscous damping coefficient in percent of critical (V_{DC}) to avoid undesirable oscillations in contact. All simulations in this study use $FS = 0.3$, $V_{DC} = 20$ and all other parameters were default. The above parameters were taken from N. Karajan et al. [15].

5.4 Calibrated parameters

A set of parameters were obtained that were capable of predicting compressive strength typical for a concrete material. These non-bonded and bonded calibrated parameters were used to create four sample models with varying particle size. Simulations on these four individual samples were studied for the predictability of bulk mechanical properties and damage behavior of concrete.

DEM particles are considered rigid and the material parameters can be assigned using key-card *MAT_RIGID. Table 11 gives the values for DEM particles. These parameters are required to calculate the stiffness values of DEM particles for non-bonded particles. Table 12 gives the values for non-bonded contact model. The parameters such as NDAMP, TDAMP, NormK and ShearK do not specify damping coefficient and spring stiffness, but are given as scale factors to their respective values. These are assigned using key-card *CONTROL_DISCRETE_ELEMENT.

The calibration simulations focus primarily on the bonded contact model parameters, as these are primarily responsible for characterizing a cementitious material such as concrete. Table 13 gives the values for bonded contact model parameters. Table 14 gives a summary of bonded contact model parameters with varying particle size, while keeping all other parameters same.

Table 11: Material parameters for DEM particles.

Parameter	Description	Value
ρ	density (kg/mm^3)	2.40E-6
E	Modulus of elasticity (GPa)	17
ν	Poisson's ratio	0.15

Table 12: Non bonded contact parameters for DEM particles.

NDAMP	TDAMP	Fric	FricR	NormK	ShearK
0.7	0.4	0.41	0.001	0.01	0.286

Table 13: Bonded contact parameters for DEM particles.

G_b (GPa)	$\bar{k}^s/\bar{k}^n$	$\bar{\sigma}_c$ (GPa)	$\bar{\tau}_c$ (GPa)	λ	α	$\bar{X}$ (mm)
320	0.7	0.5	0.25	1.0	0.2	0.01

Table 14: Calibrated bonded parameters for each sample with varying particle size.

Particle radius (mm)	G_b (GPa)	$\bar{k}^s/\bar{k}^n$	$\bar{\sigma}_c$ (GPa)	$\bar{\tau}_c$ (GPa)	λ	Total no. of particles
0.5	320	0.7	0.5	0.25	1.0	161,200
0.75	320	0.7	0.5	0.25	1.0	47,004
1.0	320	0.7	0.5	0.25	1.0	19,529
1.25	320	0.7	0.5	0.25	1.0	9,871

CHAPTER 6: RESULTS AND DISCUSSION

In this chapter, the response of a concrete cylinder due to uniaxial compressive load is studied as the particle sizes are varied. The DEM parameters used are the parameters listed in Chapter 5. The bulk mechanical properties such as strain at failure, Poisson's ratio and volumetric strains are evaluated for each sample with varying particle size. The particle size effects are discussed on these mechanical properties. Later, overall damage behavior and failure patterns on the samples are investigated.

6.1 Stress-strain curves

Uni-axial compression test is one of the most widely used methods to determine the compressive strength of concrete. Kolver K. and Roussel N. mentioned in their literature that compressive strength is the prime engineering property of concrete. A schematic of the displacement-controlled uniaxial compression of a cylinder is shown in Figure 16. If the compressive stress versus is plotted against the normal strain, the maximum stress reached is taken to be the ultimate compressive strength. When the particle size is 0.75 mm., the stress-strain curve obtained is shown in Figure 17. Engineering stress σ and strains ϵ were calculated for each of the specimen as follows:

$$\sigma = \frac{F}{A_0} \tag{29}$$

and

$$\epsilon = \frac{\delta}{L_0} \tag{30}$$

where F is the resultant force acting on top plate due to displacement loading, A_0 is the initial cross-section area normal to loading axis of the specimen, δ is the corresponding displacement of top plate in loading direction and L_0 is the initial height of the specimen.

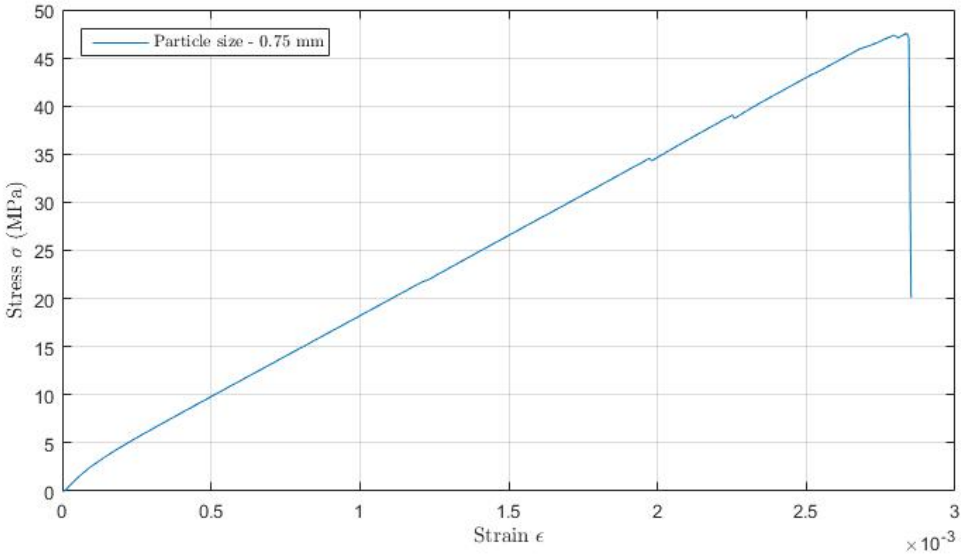

Figure 17: Engineering stress-strain curve for particle size 0.75 mm.

Gere and Timoshenko suggest that the ultimate compressive strength for plain concrete is in the range of 10 MPa to 70 MPa, with a typical value of 35 MPa [12]. Also, the Poisson's ratio is in the range of 0.1 to 0.2. Table 15 gives the bulk mechanical properties for specimen with particle size 0.75 mm. The specimen for particle size 0.75 mm is considered as the reference specimen to study the particle size effects on other bulk mechanical properties. In addition to 0.75 mm sized particles, three other particle sizes were considered for the parametric study: 0.5 mm, 1.0 mm

and 1.25 mm.

Table 15: Bulk mechanical properties for specimen with particle size 0.75 mm.

Parameter	Description	DEM simulation	Accepted range
σ_u	Ultimate compressive strength (MPa)	47.56	10-70
ϵ_c	Strain at maximum stress	0.0028	0.002-0.003
ν	Poisson's ratio	0.11	0.1-0.2

Stress-strain curves were calculated from the force-displacement curves for all four specimens with different particle sizes. Figure 18 shows the effect of particle size on engineering stress-strain curves. The stress-strain curves vary with particle size. It can be concluded from figure that as particle size increases, strain at failure increases. The decrease in strain can be explained due to the difference in packing densities of each sample. Despite using the same domain and particle generation method, a different particle size will result in a different packing density as discussed in Chapter 3. Table 16 gives the packing densities for each specimen. Also, for each sample, particles were generated from the start which led to a different particle distribution and location compared to other specimens. A lower packing density can be attributed for higher porosity. Thus, particles under load will undergo higher displacements for the same load causing larger strains in the overall bulk behavior.

Table 16: Packing densities for specimens with different particle size.

Particle size (mm)	Volume of each particle (mm^3)	Total no. of particles	Total particle volume (mm^3)	Packing density (%)
0.5	5.23E-1	161200	84404.12	53.7
0.75	1.767	47004	83062.92	52.8
1.0	4.18	19529	81802.88	52.0
1.25	8.18	9871	80756.92	51.4

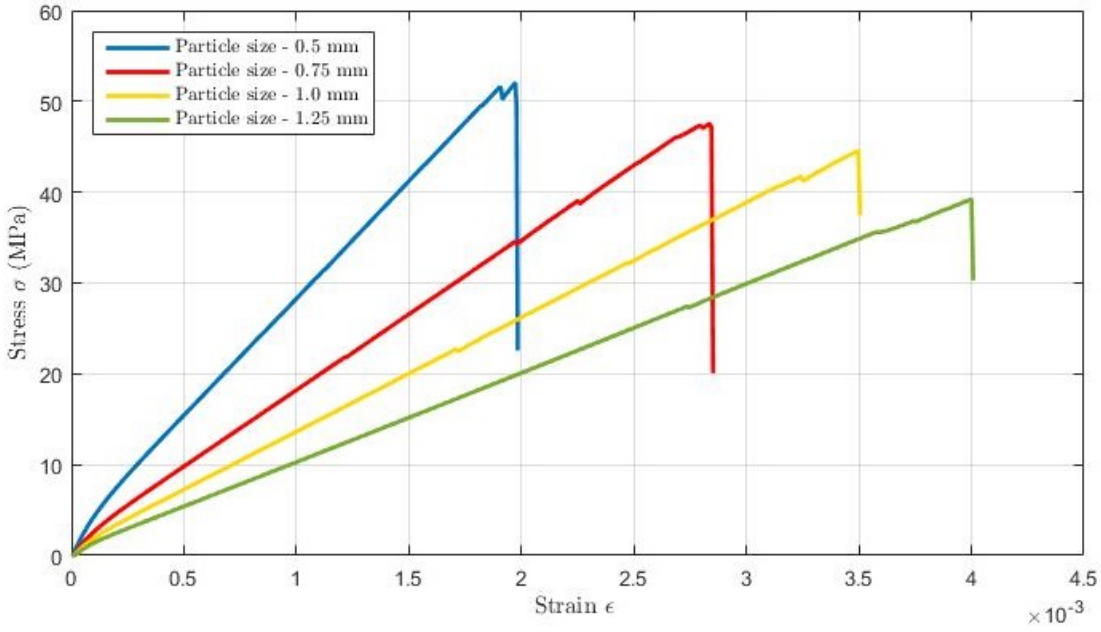

Figure 18: Engineering stress-strain curves for varying particle sizes.

The effect of particle size on maximum stress and peak strain respectively is shown in Figure 19 and Figure 20 respectively.

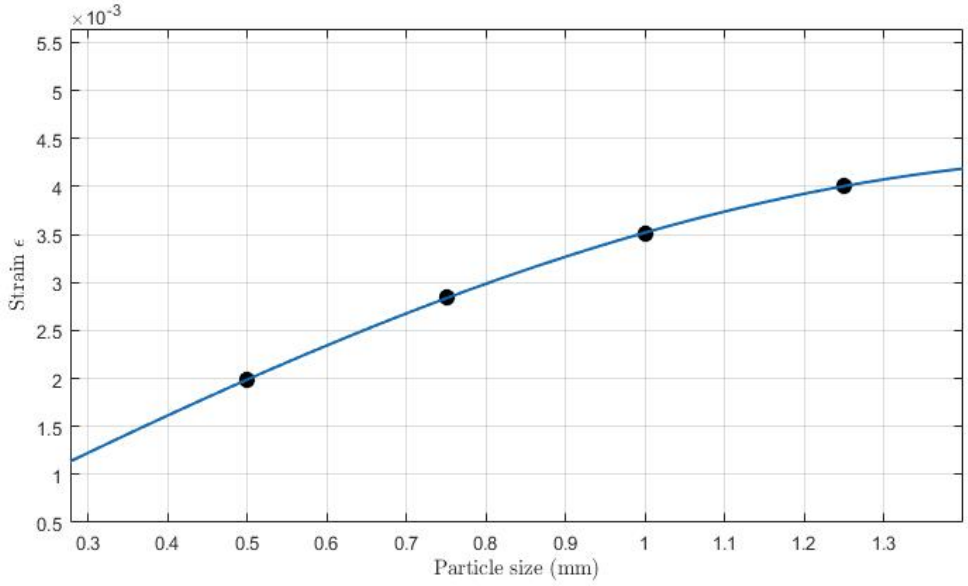

Figure 20: Effect of particle size on engineering strain.

The increase in strain due to the decrease in packing density can be validated

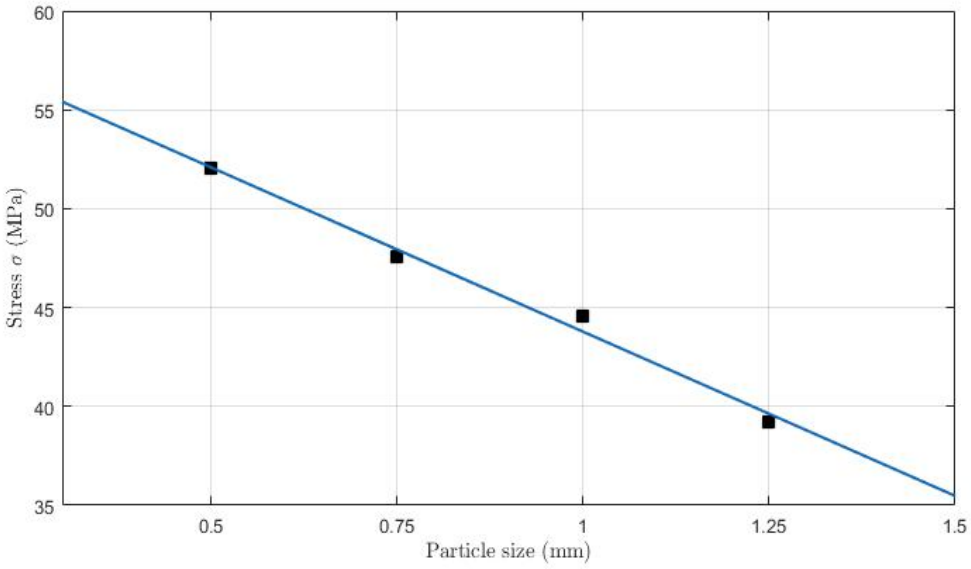

Figure 19: Effect of particle size on engineering stress.

from the domain size experiment. In this experiment, the domain size was varied while keeping the particle size same ensuring all the parameters including particle size remain same. Here, a sample of particle size 1 mm was used as reference case while reducing the domain size in percent of volume. Table 17 gives the values of domain size and its packing density. Figure 21 validates the increase in bulk strain at failure due to the decrease in packing density.

Table 17: Packing densities for specimens with varying domain size.

Domain size (height×radius) (mm)	% by volume (mm^3)	Total no. of particles	Total particle volume (mm^3)	Packing density (%)
80×25	100	19529	81802.88	52.0
72×22.5	72	14163	59325.83	51.8
65×20	52	10024	41988.43	51.4

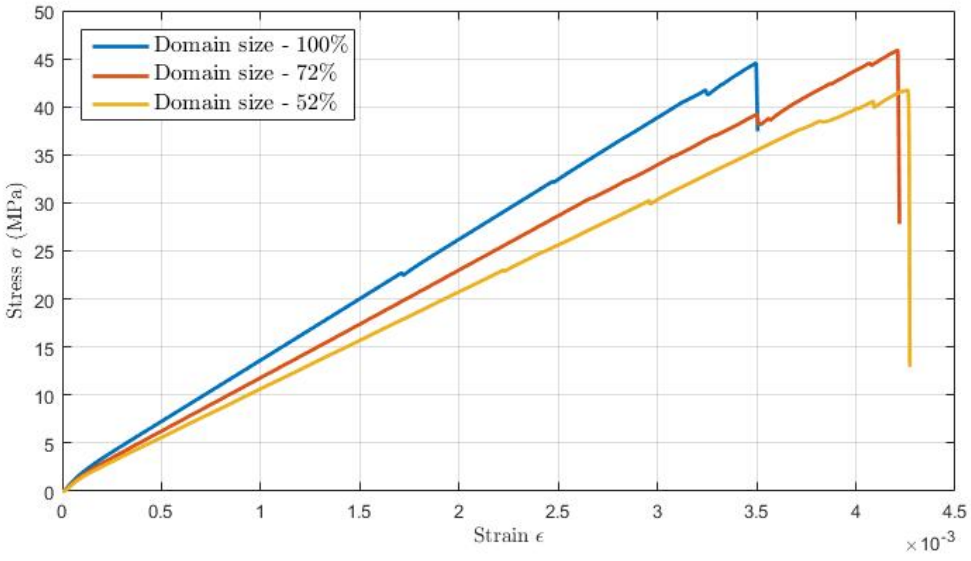

Figure 21: Effect of packing density on engineering strain at failure.

6.2 Poisson's ratio

In this study, the Poisson's ratio is calculated at 40% of maximum compressive strength. Bamforth et al. suggest that mechanical properties of concrete should be measured at approximately 30% to 40%, due to the fact that material under loading in this stage is in near elastic region [4]. The Poisson's ratio ν is the negative of the ratio of the radial strain ϵ_r to the axial strain ϵ_h:

$$\nu = -\frac{\epsilon_r}{\epsilon_h} \tag{31}$$

where the axial strain ϵ_h and radial strain ϵ_r are given by:

$$\epsilon_h = \frac{h_0 - h}{h_0} \tag{32}$$

and

$$\epsilon_r = \frac{D - D_0}{D_0}. \tag{33}$$

In these equations, h is the height of specimen, D is the average distance between diametrically outermost particles at a given z and the subscript 0 denotes initial values. Due to the random placement of particles in the domain, the two particles of a pair may not be exactly on the horizontal or vertical axis. The center line joining the particle centers may not pass through geometric center. Similarly for axial distances, the center line may not pass through geometric natural axis. To account for this, average values for D were calculated using radial distances at three different sections. The technique is further discussed in below.

6.2.1 Calculation of radial strain

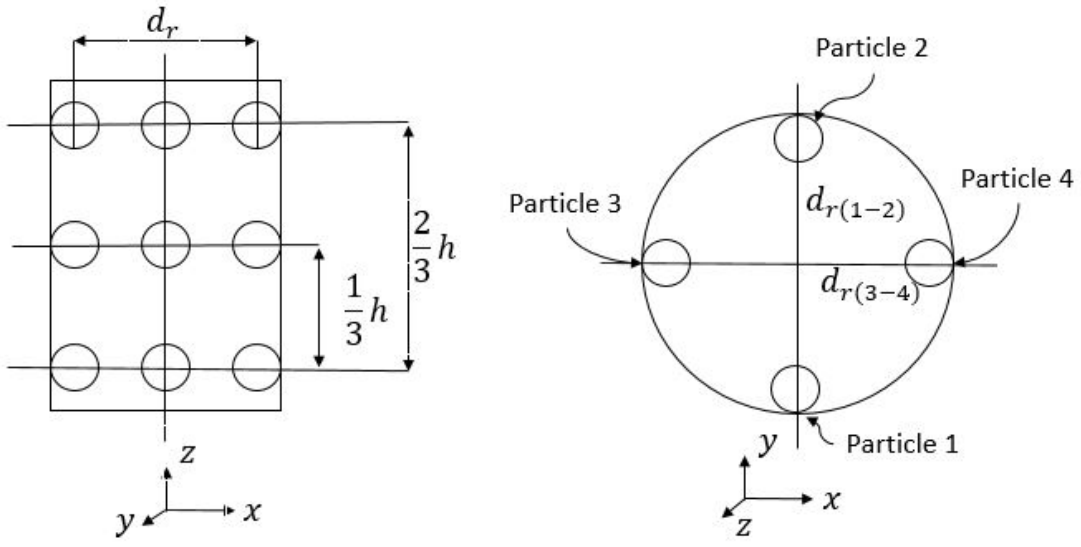

Figure 22: Schematic representation of determining average radial distance D.

Figure 22 shows the schematic representation of determining average radial distance D. The domain was divided into three sections (top-section, mid-section and bottom-

section) normal to z direction each equally spaced from mid-section. Two pairs (each pair consisting of the centers of the extremal elements on a diameter) from each section were considered for measuring D. The average distance D was then calculated as:

$$D = \frac{1}{6}\sum_{r=1}^{6} d_r \tag{34}$$

where d_r is the distance between the the centers of the extremal elements on a diameter.

6.2.2 Calculation of axial strain

The axial distance which is equal to the height of specimen was calculated similar to D, as represented in Figure 23. Though the effort was to locate the bottom most and top most particles, these particles may not be exactly on the top and bottom boundaries due to the random placement of particles.

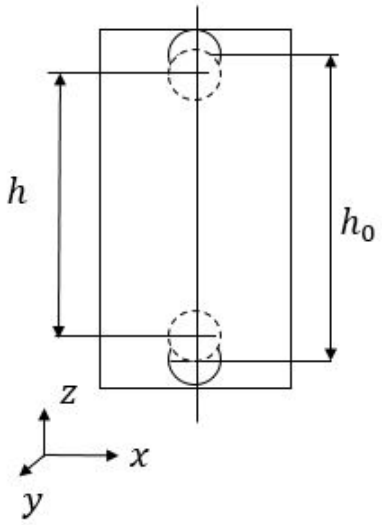

Figure 23: Schematic representation of determining axial distances h and h_0.

Table 18 gives the values for the axial, radial strains and the Poisson's ratio in

compression for all for samples. Figure 24 shows the effect of particle size on Poisson's ratio. It can be concluded that Poisson's ratio decreases only slightly with an increase in particle size. Thus, Poisson's ratio, a bulk mechanical property, can be said as dependent on parallel-bond stiffness-ratio parameter.

Table 18: Poisson's ratio for samples with varying particle size.

Particle size (mm)	Axial strain (ϵ_h)	Radial strain (ϵ_r)	Poisson's ratio (ν)
0.5	-140.01E-6	16.77E-6	0.118
0.75	-154.14E-6	17.64E-6	0.114
1.0	-174.36E-6	19.38E-6	0.111
1.25	-188.39E-6	18.29E-6	0.097

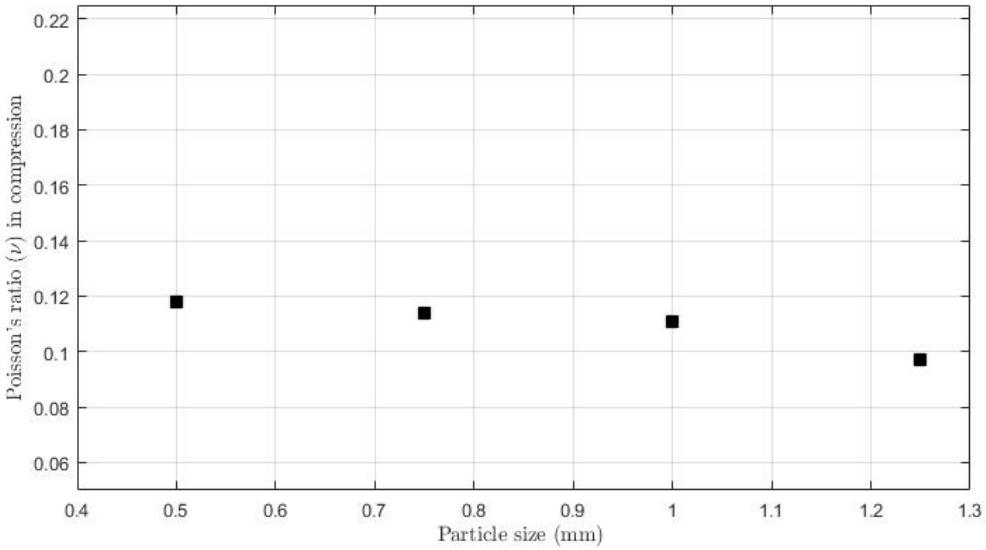

Figure 24: Effect of particle size on Poisson's ratio.

6.3 Volumetric strain

Volumetric strain e is defined as the change in volume per unit volume. For a cylindrical geometry, this can be found from:

$$e = \frac{\Delta V}{V_0} = -\epsilon_h + 2(\epsilon_{xx}) \tag{35}$$

and

$$\epsilon_{xx} = \frac{D_x - D_0}{D_0} \tag{36}$$

where ϵ_{xx} is the lateral strain in X-direction. For a uni-axial loading, the above equation gives the normal strain induced volume change. The calculation technique used here is similar as discussed in previous topic with measurements taken at three different sections. Figure 25 gives the schematic representation of determining average lateral distance D_x.

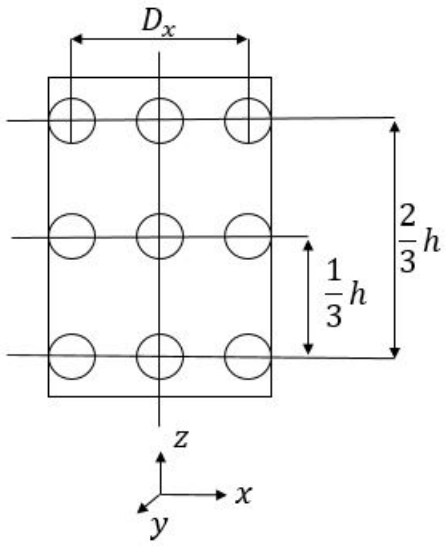

Figure 25: Schematic representation of determining average lateral distance D_x.

Figure 26 shows a plot for volumetric strain e vs. axial strain ϵ_h. The volumetric strain increases in magnitude as the axial strain increases as expected.

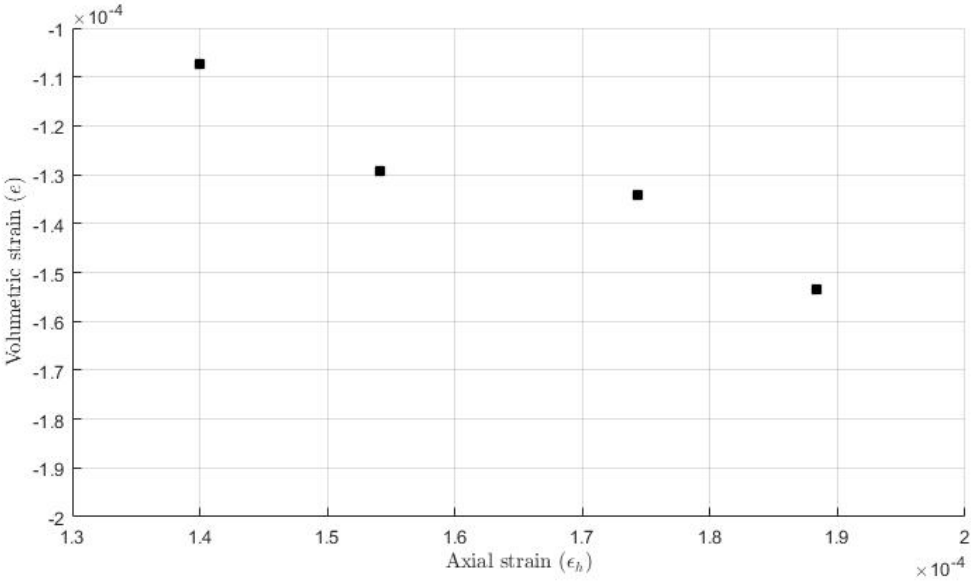

Figure 26: Volumetric strain vs. axial strain.

6.4 Failure pattern

Mindess et al. *Concrete* discuss the typical patterns observed in the failure of concrete under uniaxial compression loading [19]. They also discuss the influence of friction between test specimen and loading plates. According to them, the friction between the plates and specimen limits the radial expansion of material under loading and thus resulting in cracks propagating at the top and bottom surface at an angle while propagating vertically in the center. This results in a well formed cones at the ends. Figure 27 shows a typical failure patterns observed in concrete cylinders under uni-axial loading.

All simulations in this work were performed with friction between plates and specimen. With DEM simulations, the phenomena of crack propagation and failure can be well studied by visualizing contour plots for broken bonds. However LS-PrePost V4.3, does not provide the ability to visualize broken bonds between bonded particles.

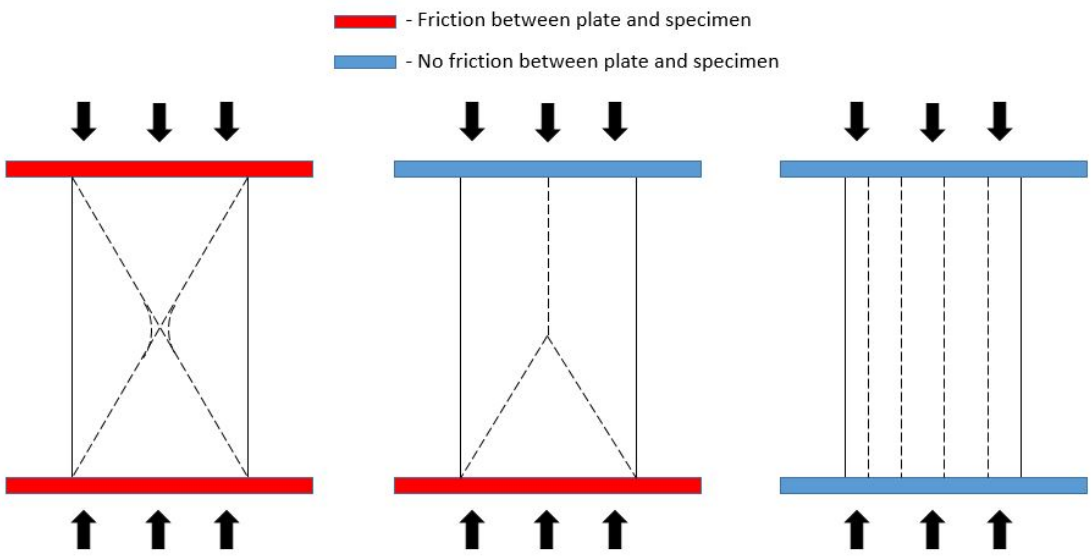

Figure 27: Typical failure patterns observed in concrete cylinder under uni-axial loading. (Adapted from [19])

With contour plots for axial and lateral displacements of particles at mid-section of the specimen, it can be visualized for shearing planes and eventual failure patterns. As evident in Figures (28- 31), the specimens with particle sizes 0.5 mm and 0.75 mm show a well formed cone shapes at both the ends. This is in complete agreement with the observations made by Mindess et al. However, for particle sizes 1.0 mm and 1.25 mm, as shown in Figures (32- 35), the conical shapes do form but are not as well developed as they are for the smaller particle sizes. Furthermore, in these cases, diagonal cracking is observed. Thus, it can be concluded that the particle size and packing density influence the failure patterns observed in the simulations.

The following shows contour plots of particle displacement for each of four calibrated samples.

6.4.1 Failure pattern for specimen with particle size of 0.5 mm

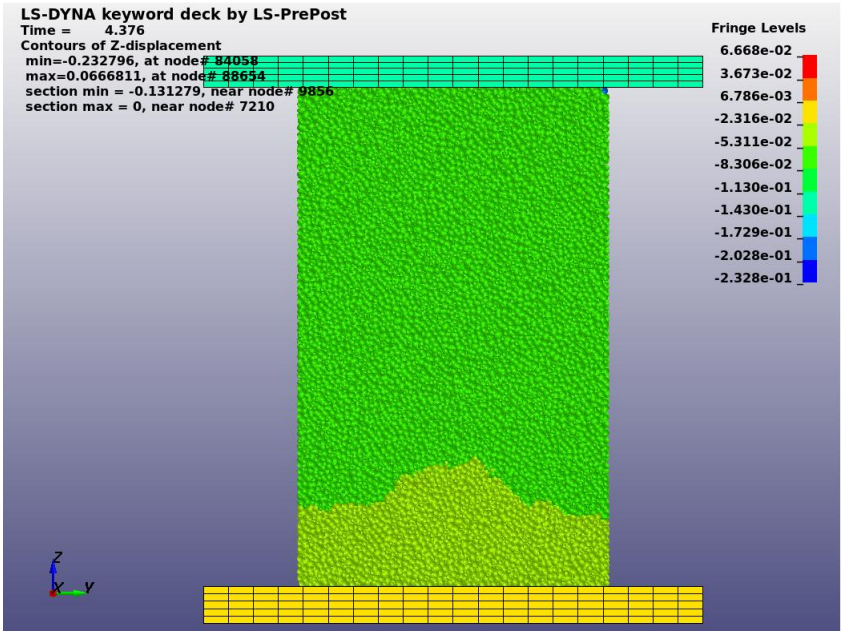

Figure 28: Contour plots for axial displacements (Particle size - 0.5 mm).

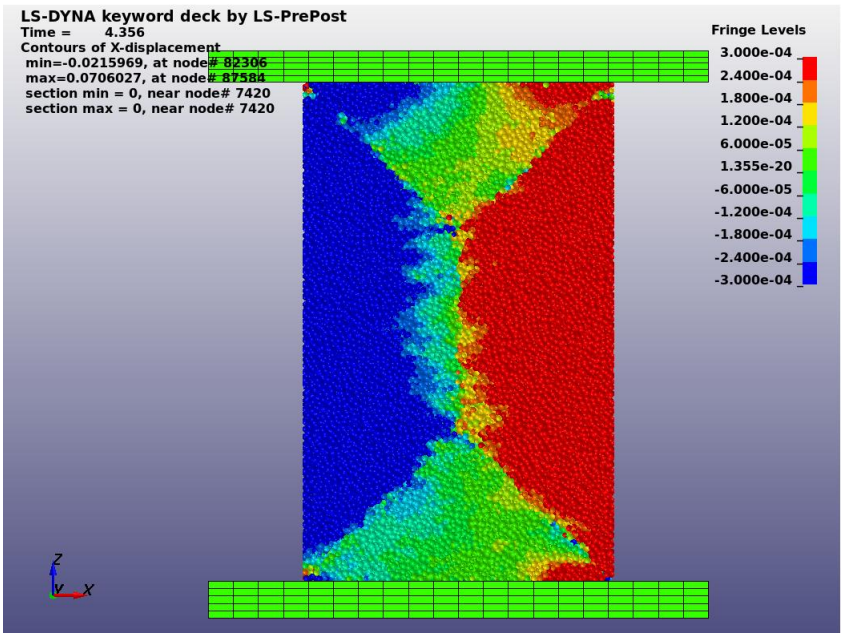

Figure 29: Contour plots for lateral displacements (Particle size - 0.5 mm).

6.4.2 Failure pattern for specimen with particle size of 0.75 mm

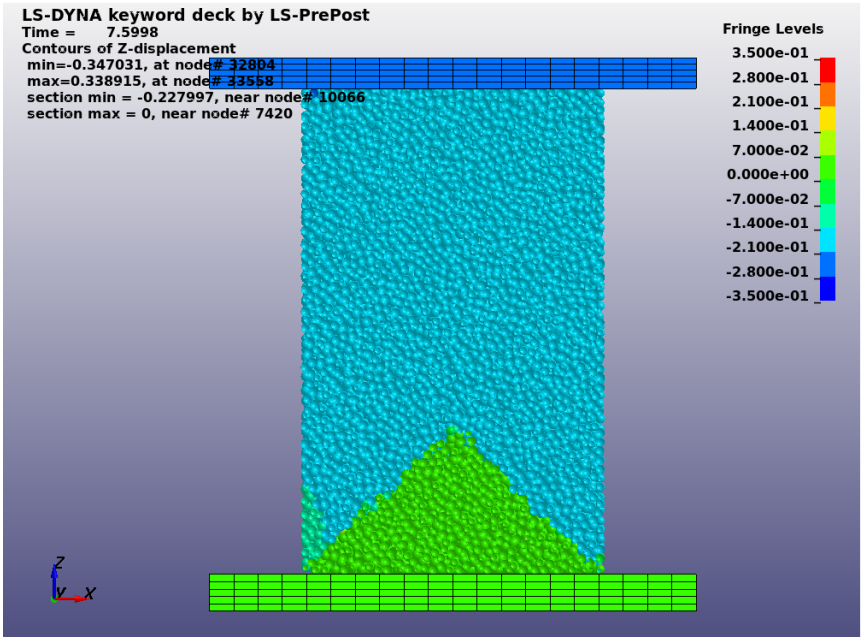

Figure 30: Contour plots for axial displacements (Particle size - 0.75 mm).

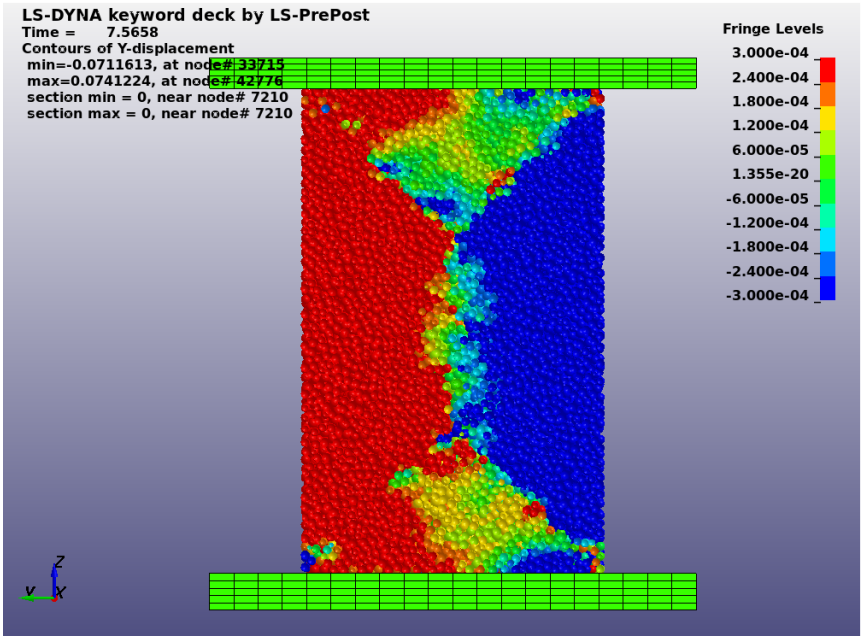

Figure 31: Contour plots for lateral displacements (Particle size - 0.75 mm).

6.4.3 Failure pattern for specimen with particle size of 1.0 mm

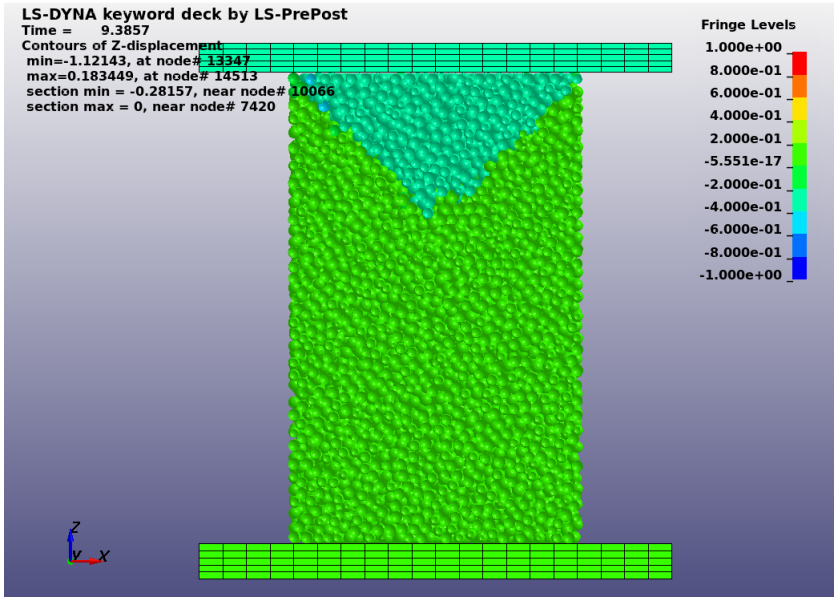

Figure 32: Contour plots for axial displacements (Particle size - 1.0 mm).

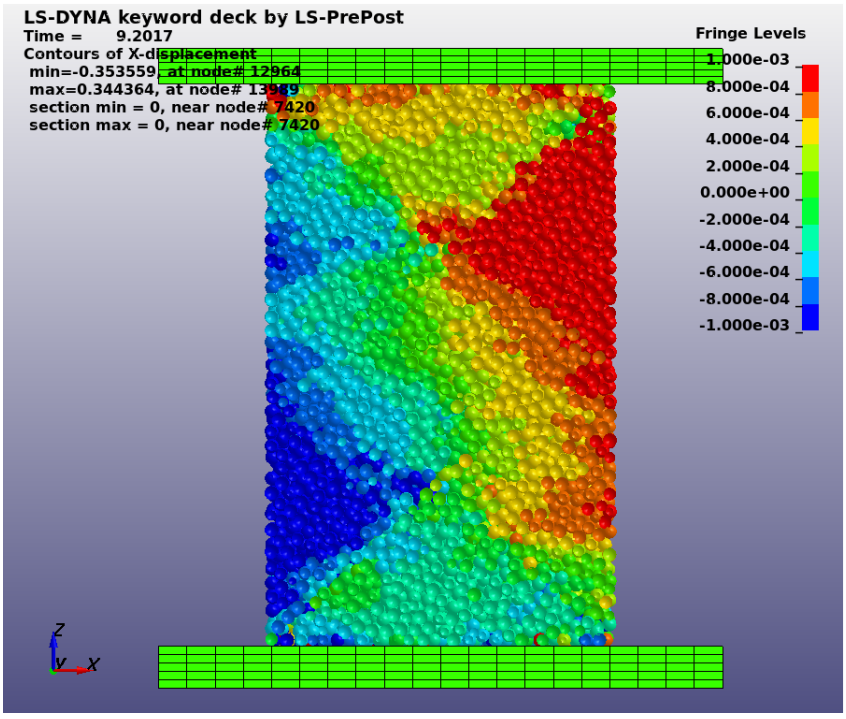

Figure 33: Contour plots for lateral displacements (Particle size - 1.0 mm).

6.4.4 Failure pattern for specimen with particle size of 1.25 mm

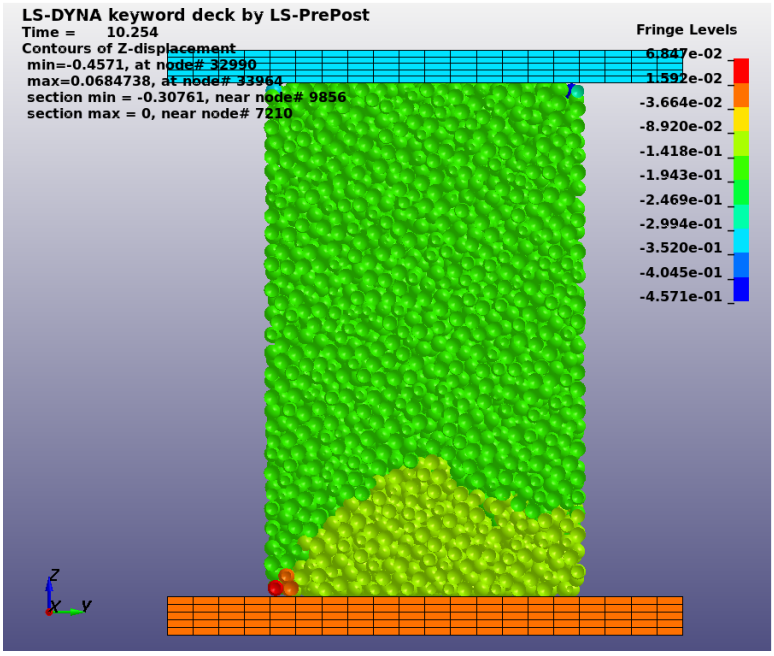

Figure 34: Contour plots for axial displacements (Particle size - 1.25 mm).

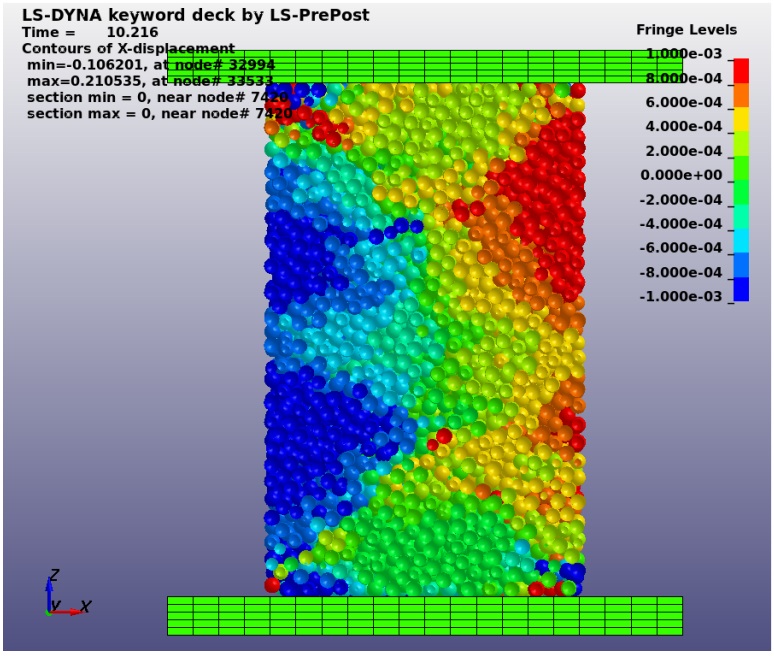

Figure 35: Contour plots for lateral displacements (Particle size - 1.25 mm).

CHAPTER 7: CONCLUSIONS AND RECOMMENDATIONS FOR FUTURE WORK

7.1 Conclusions

Based on the results presented in the previous chapters, the following conclusions can be drawn. With proper calibration and the use of bonded particle method as an additional contact model incorporated in conventional DEM, it can be concluded that DEM can be successfully used to model cementitious materials like concrete. Bonded-Particle DEM also particularly successfully captured the failure pattern as observed in concrete material due to its inherent homogeneity in the model. The failure patterns were in close agreement with the literature discussed by Mindess et al. and all the samples show a unanimous representation of the expected failure pattern that is the failure pattern for friction between plates and specimen.

The use of simpler models like two-particle and three-particle, can be successfully used to calibrate larger and complex models. Satisfactory results were achieved for all the key mechanical properties in all four samples as observed in literature.

The bulk response of the material appears to depend on the particle size and packing density. Therefore, caution must be exercised in deriving bulk properties based on DEM analyses. Further work is needed to understand optimal particle sizes and packing densities for accurately predicting the bulk response of concrete. Particle size is one of the major parameter that affects the overall bulk behaviour; however, a

smaller particle size is desired to achieve better resolution of crack propagation and failure pattern.

7.2 Recommendations for future work

This thesis demonstrates the modeling of concrete material under uni-axial loading using a bonded particle method. Although this research mainly focuses on the uni-axial loading of a concrete cylinder and the influence of bonded contact parameters, there are several areas of research which could further improve the current model's capabilities.

The parametric study was limited to four most fundamental bonded-contact parameters and their influence on DEM behavior. Further studies on the influence of the remaining bond parameters such as the bond radius multiplier λ and the distance between two bonded particles $\bar{X}$ would have made the parametric study more comprehensive.

Particle distribution in the DEM model was limited to a mono-disperse method where all the particles considered were of the same size. A study using poly-disperse method would help understand the influence of non uniformly distributed particle sizes on the bulk response of the model. In addition, if the particle size ratios are closely matched with a realistic material, the poly-disperse model could potentially lead to more insights into the damage and failure patterns of the material.

Another extension of the studies presented in this work would be to develop DEM models for triaxial compression and Brazilian tests. These models would further help understand the response and failure of concrete structures.

REFERENCES

[1] The origins of the finite element method, http://www.colorado.edu/engineering/CAS/courses.d/IFEM.d/IFEM.AppO.d/IFEM.AppO.pdf. (Accessed on 19/05/2017).

[2] *Concrete through the ages*. British Cement Association, 1999.

[3] B. Aresh. *Fundamental Study into the Mechanics of Material Removal in Rock Cutting*. PhD thesis, Northumbria University, 2012.

[4] P. Bamforth, D. Chisholm, J. Gibbs, and T. Harrison. Properties of concrete for use in euro code 2. *The Concrete Centre, UK*, 2008.

[5] N. J. Brown. *Discrete element modelling of cementitious materials*. PhD thesis, The University of Edinburgh, 2013.

[6] H. A. Carmona, F. K. Wittel, F. Kun, and H. Herrmann. Fragmentation processes in impact of spheres. *Physical Review E*, 77(5):051302, 2008.

[7] P. A. Cundall. A computer model for simulating progressive, large-scale movements in blocky rock system. In *Proc. Int. Symp. for ISRM, Nancy, Paper*, number 8, 1971.

[8] P. A. Cundall and R. D. Hart. Numerical modelling of discontinua. *Engineering Computations*, 9(2):101–113, 1992.

[9] P. A. Cundall and O. D. Strack. A discrete numerical model for granular assemblies. *Geotechnique*, 29(1):47–65, 1979.

[10] C. Ergenzinger, R. Seifried, and P. Eberhard. A discrete element model to describe failure of strong rock in uniaxial compression. *Granular Matter*, 13(4):341–364, 2011.

[11] Y. Feng, K. Han, and D. Owen. An advancing front packing of polygons, ellipses and spheres. In *Discrete Element Methods: Numerical Modeling of Discontinua*, pages 93–98. 2002.

[12] J. Gere and S. Timoshenko. Mechanics of materials, 2nd edn (monterey, ca: Brooks/cole engineering division). 1984.

[13] Z. Gyurkó, K. Bagi, and A. Borosnyói. Discrete element modelling of uniaxial compression test of hardened concrete. *Építöanyag (Online)*, (4):113, 2014.

[14] D. Hallbauer, H. Wagner, and N. Cook. Some observations concerning the microscopic and mechanical behaviour of quartzite specimens in stiff, triaxial compression tests. In *International Journal of Rock Mechanics and Mining Sciences & Geomechanics Abstracts*, volume 10, pages 713–726. Elsevier, 1973.

[15] N. Karajan, E. Lisner, Z. Han, H. Teng, and J. Wang. Particles as discrete elements in ls-dyna: interaction with themselves as well as deformable or rigid structures. In *11th LS-DYNA Forum, Ulm*, 2012.

[16] J. M. Kemeny and N. G. Cook. Micromechanics of deformation in rocks. In *Toughening mechanisms in quasi-brittle materials*, pages 155–188. Springer, 1991.

[17] H. Kim and W. G. Buttlar. Discrete fracture modeling of asphalt concrete. *International Journal of Solids and Structures*, 46(13):2593–2604, 2009.

[18] S. Liu, D. Sun, and Y. Wang. Numerical study of soil collapse behavior by discrete element modelling. *Computers and Geotechnics*, 30(5):399–408, 2003.

[19] S. Mindess, J. F. Young, and D. Darwin. *Concrete*. Prentice Hall, 2003.

[20] R. Mindlin and H. Deresiewicz. Timoshenko's shear coefficient for flexural vibrations of beams. Technical report, DTIC Document, 1953.

[21] T. Moon, M. Nakagawa, and J. Berger. Measurement of fracture toughness using the distinct element method. *International Journal of Rock Mechanics and Mining Sciences*, 44(3):449–456, 2007.

[22] P. R. Nayak. Surface roughness effects in rolling contact. *Journal of Applied Mechanics*, 39(2):456–460, 1972.

[23] M. Nitka and J. Tejchman. Modelling of concrete behaviour in uniaxial compression and tension with dem. *Granular Matter*, 17(1):145–164, 2015.

[24] B. Park and K.-B. Min. Bonded-particle discrete element modeling of mechanical behavior of transversely isotropic rock. *International Journal of Rock Mechanics and Mining Sciences*, 76:243–255, 2015.

[25] A. Potapov and C. Campbell. Two mechanisms of particle impact breakage. *Metal Powder Report*, 6(53):34–35, 1998.

[26] D. Potyondy and P. Cundall. A bonded-particle model for rock. *International Journal of Rock Mechanics and Mining Sciences*, 41(8):1329–1364, 2004.

[27] J. Rojek. Discrete element modelling of rock cutting. *Computer Methods in Materials Science*, 7:224–230, 2007.

[28] B. Schneider, M. Bischoff, and E. Ramm. Modeling of material failure by the discrete element method. *PAMM*, 10(1):685–688, 2010.

[29] T. Tsuji, Y. Nakagawa, N. Matsumoto, Y. Kadono, T. Takayama, and T. Tanaka. 3-d dem simulation of cohesive soil-pushing behavior by bulldozer blade. *Journal of Terramechanics*, 49(1):37–47, 2012.

[30] P. Wang and C. Arson. Discrete element modeling of shielding and size effects during single particle crushing. *Computers and Geotechnics*, 78:227–236, 2016.

[31] M. Yao and A. Anandarajah. Three-dimensional discrete element method of analysis of clays. *Journal of Engineering Mechanics*, 129(6):585–596, 2003.

[32] Z. You, S. Adhikari, and Q. Dai. Three-dimensional discrete element models for asphalt mixtures. *Journal of Engineering Mechanics*, 134(12):1053–1063, 2008.

[33] H. Zhu, Z. Zhou, R. Yang, and A. Yu. Discrete particle simulation of particulate systems: theoretical developments. *Chemical Engineering Science*, 62(13):3378–3396, 2007.